The quench control of water estimates in convergent margin magmas

MAXIM GAVRILENKO^{1,2,*,†}, MICHAEL KRAWCZYNSKI¹, PHILIPP RUPRECHT², WENLU Li^{3,‡}, AND JEFFREY G. CATALANO¹

¹Department of Earth and Planetary Sciences, Washington University in St. Louis, Campus Box 1190, One Brookings Drive, St. Louis, Missouri 63130, U.S.A. Orcid 0000-0002-0710-0763.

²Department of Geological Science and Engineering, University of Nevada, Reno, 1664 N. Virginia Street, Reno, Nevada 89557, U.S.A. ³Department of Energy, Environmental, and Chemical Engineering, Washington University in St. Louis, Campus Box 1180, One Brookings Drive, St. Louis, Missouri 63130, U.S.A.

ABSTRACT

Here we present a study on the quenchability of hydrous mafic melts. We show via hydrothermal experiments that the ability to quench a mafic hydrous melt to a homogeneous glass at cooling rates relevant to natural samples has a limit of no more than 9 ± 1 wt% of dissolved H₂O in the melt. We performed supra-liquidus experiments on a mafic starting composition at 1-1.5 GPa spanning H₂Oundersaturated to H₂O-saturated conditions (from ~1 to ~21 wt%). After dissolving H₂O and equilibrating, the hydrous mafic melt experiments were quenched. Quenching rates of 20 to 90 K/s at the glass transition temperature were achieved, and some experiments were allowed to decompress from thermal contraction while others were held at an isobaric condition during quench. We found that quenching of a hydrous melt to a homogeneous glass at quench rates comparable to natural conditions is possible at water contents up to 6 wt%. Melts containing 6-9 wt% of H₂O are partially quenched to a glass, and always contain significant fractions of quench crystals and glass alteration/devitrification products. Experiments with water contents greater than 9 wt% have no optically clear glass after quench and result in fine-grained mixtures of alteration/devitrification products (minerals and amorphous materials). Our limit of 9 ± 1 wt% agrees well with the maximum of dissolved H₂O contents found in natural glassy melt inclusions (8.5 wt% H₂O). Other techniques for estimating pre-eruptive dissolved H₂O content using petrologic and geochemical modeling have been used to argue that some arc magmas are as hydrous as 16 wt% H₂O. Thus, our results raise the question of whether the observed record of glassy melt inclusions has an upper limit that is partially controlled by the quenching process. This potentially leads to underestimating the maximum amount of H₂O recycled at arcs when results from glassy melt inclusions are predominantly used to estimate water fluxes from the mantle.

Keywords: Mafic glassy melt inclusions, hydrous mafic glass quenchability, arc volatile budget, magmatic water; Applications of Fluid, Mineral, and Melt Inclusions

INTRODUCTION

Arc magmas are almost exclusively hydrous (e.g., Sobolev and Chaussidon 1996; Wallace 2005; Métrich and Wallace 2008; Plank et al. 2013; Zellmer et al. 2015) as a result of subducting slab dehydration (Sobolev and Chaussidon 1996; Kamenetsky et al. 2002; Grove et al. 2006). The maximum dissolved H₂O content in magmas plays a pivotal role in the generation (Katz et al. 2003; Grove et al. 2006, 2012) and evolution (Grove et al. 2003, 2012; Zimmer et al. 2010) of arc melts. Within the crust, magma transport and eruption is strongly modulated by dissolved H₂O since it imparts buoyancy to primitive magmas traveling through the crust (Herzberg et al. 1983; Ochs and Lange 1999; Carmichael 2002), and when H₂O exsolves at shallow pressures, it affects explosivity through volumetric expansion (Cashman

2004). Besides the effects of H₂O on the magmatic system itself,

Currently, magmatic H₂O content estimations are based mostly on studies of melt inclusions (e.g., Sobolev and Chaussidon 1996; Kamenetsky et al. 1997; Frezzotti 2001; Danyushevsky et al. 2002; Kamenetsky et al. 2002; Schiano 2003; Kent 2008); in particular, melt inclusions that are glassy and hosted by the most magnesian olivine crystals, present in tephra/scoria. Melt inclusions (MIs) act as tiny pressure capsules potentially preserving the chemistry of pristine primitive melts as well as minimum dissolved H₂O contents. The physical state of MIs post entrapment can be thought of as having three major end-members: (1) glassy MIs; (2) crystallized MIs; and (3) devitrified MIs. The resulting type of the MI strongly depends on its cooling rates (Anderson

the $\rm H_2O$ budget in convergent margins affects mantle rheology and geophysical parameters like seismic wave speed, attenuation, and conductivity of the lithosphere and mantle (Hacker et al. 2003; Pozgay et al. 2009; McGary et al. 2014). Because water plays such a central role in magma genesis and evolution at convergent margins, knowing the water content of the most primitive magma samples at volcanic arcs is of first-order importance.

^{*} E-mail: gavrilenko.maxim@wustl.edu

[‡] Present address: Department of Chemical and Environmental Engineering, Yale University, 17 Hillhouse Avenue, New Haven, CT 06520, U.S.A.

[†] Special collection papers can be found online at http://www.minsocam.org/MSA/AmMin/special-collections.html.

1991; Frezzotti 2001). Because it has long been assumed that the glassy single-phase melt inclusions have the most rapid cooling rates, direct secondary ion mass spectrometer (SIMS) and Fourier-transform infrared spectroscopy (FTIR) measurements of H₂O dissolved in *glassy* MIs have served for decades as the "gold standard" for determining magmatic pre-eruptive H₂O content (e.g., Wallace 2005; Plank et al. 2013). *Crystallized* MIs are thought to be produced during slow cooling (Skirius et al. 1990; Anderson 1991; Frezzotti 2001) and thus are usually presumed to be subject to diffusive degassing of H₂O in nature. These inclusions are rarely used for volatile species studies (e.g., Skirius et al. 1990; Esposito et al. 2016). *Devitrified* MIs are the result of partial modification of the glass, and those melt inclusions are usually discarded by researchers of magmatic volatile species (Kent 2008).

While the evolution of magmatic H₂O at shallow depths has been studied thoroughly using glassy MI (e.g., Wallace 2005; Plank et al. 2013), the evolution of magmatic H₂O in deeper parts of subduction zones remains less constrained. Volatile-rich magmas undergo nearly complete degassing during ascent, eruption, and cooling. Because H₂O solubility is pressure dependent (e.g., Moore et al. 1998; Papale et al. 2006; Shishkina et al. 2010; Mitchell et al. 2017), high water contents above 9 wt% would require MIs to have formed at mid to lower crustal or even upper mantle pressures, but no mafic glassy melt inclusions preserving >9 wt% H₂O have been found (Fig. 1). The existence and preservation of such melt inclusions are further challenged by the fact that hydrogen diffusion through the crystal lattice of the host allows equilibration between the degassing matrix melt and the entrapped pressurized melt droplet. Recent studies have demonstrated that hydrogen diffusion within a host mineral is rapid (Danyushevsky et al. 2002; Hauri 2002; Portnyagin et al. 2008; Chen et al. 2011; Gaetani et al. 2012; Bucholz et al. 2013; Lloyd et al. 2013; Hartley et al. 2015), causing MIs to be partially open to lose (or gain) volatile species. Hydrogen may also migrate along dislocations or propagation of defect points in the host mineral (Massare et al. 2002; Portnyagin et al. 2008), further enhancing hydrogen exchange between the melt inclusion and the matrix melt. Thus, it has been acknowledged that the amount of H₂O that MIs contain likely represents a minimum from what was originally dissolved in a particular magma (Gaetani and Watson 2000; Danyushevsky et al. 2002; Hauri 2002; Portnyagin et al. 2008; Gaetani et al. 2012; Bucholz et al. 2013; Lloyd et al. 2013).

Despite the limitations in the use of glassy melt inclusions, they are still assumed to be among the best archives to record preeruptive primitive water contents (e.g., Sobolev and Chaussidon 1996; Kamenetsky et al. 1997; Kamenetsky et al. 2002; Wallace 2005; Plank et al. 2013; Wallace et al. 2015b), especially when quenched rapidly as tephra of mafic magmas. The rapid quench of the melt inclusions upon eruption, or even before eruption, results in the preservation of the melt inside host minerals as clear glass. Melt inclusions from primitive olivine phenocrysts in tephra and scoria are assumed to best preserve the pre-eruptive water contents of melts with a mantle origin, so these samples are preferentially analyzed. The highest amount of water recorded in melt inclusions with mafic compositions is ~8.5 wt% (de Moor et al. 2013) hosted in minerals from nephelinitic magmas, related to rift settings. In arc settings the maximum is slightly

lower at 7.0–7.5 wt% of H_2O (Auer et al. 2009; Zimmer et al. 2010; Weller and Stern 2018).

Many excellent MI studies have significantly improved our understanding of the H₂O variations in arc magmas (e.g., review/summary in Wallace 2005; Kent 2008; Plank et al. 2013). A review of the existing database of inclusions that have been quantitatively studied for their dissolved H₂O contents concluded that the maximum H₂O content in melt inclusions from a single volcano or cinder cone ranges typically between 1–7 wt% (Plank et al. 2013). Those researchers (Plank et al. 2013) and other studies (Gaetani and Watson 2000; Danyushevsky et al. 2002; Hauri 2002; Portnyagin et al. 2008; Gaetani et al. 2012; Bucholz et al. 2013; Lloyd et al. 2013) have recognized the open system behavior of MIs. Nonetheless, it is still generally interpreted that the maximum water contents of MIs in primitive magmas in subduction zone settings are representative of the amount of H₂O in primitive arc melts (e.g., Straub and Layne 2003; Wallace 2005; Moore 2008; Parai and Mukhopadhyay 2012; Wallace et al. 2015b; Peslier et al. 2017).

An alternative interpretation of the maximum water content found in glassy melt inclusions is that melts with higher water contents do not quench to a homogeneous glass at natural quenching rates. Such higher water contents (14-16 wt%) for arc magmas have been postulated, based on other petrologic constraints, to exist at the deep crust and upper mantle conditions (Carmichael 2002; Fischer and Marty 2005; Krawczynski et al. 2012). The fact that the majority (98%) of studied glassy MIs record last equilibration at shallow pressures (<500 MPa; Wallace 2005) raises the question whether all MIs formed and/or equilibrated at shallow depths, or whether MIs are formed at all pressures, but by selectively analyzing glassy samples there is a bias in the current data set to low H₂O melt inclusions or those that formed or re-equilibrated shallowly. Here we show that the low-pressure record in MIs is not only a result of shallow entrapment or re-equilibration on the ascent, but potentially also due to the ability of quenched glass to retain H₂O in its structure when it is formed as the hydrous silicate melt passes the glass transition.

Here we define the term "quenchability," which refers to the ability of a silicate melt to be transformed to a glass upon cooling. This kinetically driven process strongly depends on such parameters as degree of melt polymerization and cooling rates (Dingwell and Webb 1990). Adding a significant amount of H_2O to a melt lowers the glass transition temperature (T_2) , potentially making hydrous melts harder to quench and producing non-glassy melt inclusions. Devitrified or crystallized MIs are preferentially not studied for their volatile content. Below we present evidence that if hydrous mafic magmas contain greater than ~9 wt% H₂O they cannot form glassy MIs at naturally occurring quench rates. Studies that make global calculations of water exchange between the Earth's interior and the exosphere using MI data for estimates of H₂O contents in arc magmas (e.g., Hacker 2008; van Keken et al. 2011; Parai and Mukhopadhyay 2012), are likely underestimating the amount of recycled H₂O in some sub-arc settings. In addition, recent geophysical studies show that the amount of subducted water may be much higher than previously realized (Cai et al. 2018), which would require some amount of arc magmas to contain higher water contents than traditionally recognized.

EXPERIMENTAL APPROACH

The MI record stands in contrast to studies using petrologic and geochemical proxies that provide evidence for up to 16 wt% of H₂O in some arc magmas (Carmichael 2002; Fischer and Marty 2005; Krawczynski et al. 2012). An underlying assumption in MI studies is that glassy MIs (single phase ± a single exsolution bubble) have the best chance to faithfully record pre-eruptive H₂O content, while non-glassy MIs (multiple phases) are commonly interpreted as potentially slowly cooled (and, thus, have experienced more H₂O degassing by diffusion) and also require additional stages of sample preparation (e.g., Skirius et al. 1990; Esposito et al. 2016). Anecdotally, many previous experimental studies involving H₂O-bearing silicate melts have reported problems with quenching mafic glasses with a high water content of more than 8 wt% of H₂O (e.g., Grove et al. 2006; Behrens et al. 2009; Baker and Alletti 2012; Shishkina 2012). However, the quenchability limit for hydrous silicate melts has not been studied systematically before. This then begs the question: how much water can we quench in a single-phase mafic glassy inclusion with naturally occurring cooling rates?

To test the limits of quenchability for hydrous glasses for naturally occurring cooling rates, we conducted a series of hydrous (1-21 wt% of pre-loaded H₂O) supra-liquidus temperature experiments (1225-1300 °C, 1-1.5 GPa) on a mafic calc-alkaline composition (Table 1), to determine the highest concentration of dissolved H2Ototal that a quenched glass is able to contain (H₂O_{total} accounts for all hydrogen species in the glass). The mafic composition for experiments was chosen because previous studies have explored primitive magma water contents in the mafic range of 44-56 wt% SiO₂ (Fig. 1). Synthetic glass powders and deionized water were loaded in Au₈₀Pd₂₀ metal capsules and heated above the liquidus and equilibrated for 10–16 h in a piston-cylinder apparatus. The experiments were heated to 1225–1300 °C, near or above the liquidus (depending on the water content), and quenched at rates applicable to cooling rates for volcanic tephra (Lloyd et al. 2013) (see Materials and Methods section for more details). Dissolved H₂O contents in quenched experimental run products were determined by thermo-gravimetric analysis (TGA), electron microprobe analysis (EPMA; "volatiles by difference" method), and secondary ion mass spectrometry (SIMS).

The experimental pressure (1–1.5 GPa) represents deep crustal and shallow mantle pressures. We have chosen this pressure because $\rm H_2O$ solubility in the melt is sufficiently high (~16–20 wt% $\rm H_2O$; e.g., Shishkina et al. 2014; Mitchell et al. 2017 and references therein) to contain far more dissolved $\rm H_2O$ than what is recorded in natural glassy MIs (Fig. 1). Overall, $\rm H_2O$ solubility in melts/glasses of different compositions has been best constrained at conditions \leq 500 MPa representing crustal depths shallower than 15–16 km (Hamilton et al. 1964; Moore et al. 1998; Papale et al. 2006; Shishkina et al. 2010 and others).

MATERIALS AND METHODS

Starting materials

Experiments were conducted on a starting composition that was synthesized to match the composition of a primitive basaltic andesite (Mg# = 71), 85–44, erupted from Mt. Shasta, California, in the Cascades (Baker et al. 1994; Grove et al. 2003, 2005). This basaltic andesite was chosen because it is a low silica (52 wt% SiO₂), high MgO (10.5 wt% MgO) end-member of the Mt. Shasta primitive lava suite, and known from experimental studies to be a hydrous magma composition. The starting composition was made from reagent-grade oxides and carbonates, ground under isopropanol in a ball mill, and decarbonated at 1000 °C for 8 h. The ground powder was held at 1500 °C in a Pt crucible in air for 1 h, and then quenched to a glass by dropping the crucible in water. The glass was extracted from the crucible and ground in an agate mortar under isopropanol. The ground glass was then remelted in air and quenched and crushed following the same procedures to ensure homogeneity. In total, the melting/grinding procedure was repeated three times to ensure a homogeneous and crystal-free starting material. The major element composition and homogeneity

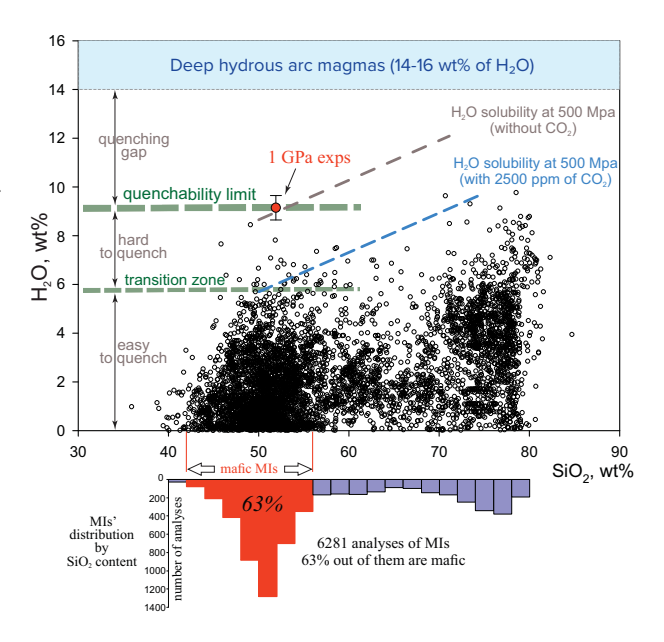


FIGURE 1. Measured H₂O variations in melt inclusions with different bulk compositions. Major element compositions of the melt inclusions are normalized to an anhydrous basis, and SiO₂ is plotted. H₂O concentrations range up to 8-9 wt% (bold dashed green line). Experimental results showing the maximum possible H₂O content in a mafic glass (this study) are shown with a red circle (1σ error bars). Quenched glassy melt inclusions have not been found with the high water contents (14-16 wt% H₂O) previously estimated by petrological and geochemical studies (Carmichael 2002; Fischer and Marty 2005; Krawczynski et al. 2012). Dashed gray and blue lines are H₂O solubility limits for 500 MPa having no CO₂ (gray line) and having 2500 ppm of CO₂ provided by the model reported in Shishkina et al. (2014). MI data (6300 analyses) are from the GEOROC database (Geochemistry of rocks of the Oceans and Continents; MPI für Chemie, Mainz, Germany, http://georoc.mpch-mainz.gwdg.de/georoc). The histogram at the bottom panel illustrates the distribution of studied MIs by SiO₂ content showing the abundance of mafic MIs in the global compilation due to numerous studies of primitive magmas.

TABLE 1. Glass starting material for experiments in oxide weight percents measured by EPMA

					<i>J</i> 1							
Starting material	n	SiO ₂ ^a	TiO ₂	Al ₂ O ₃	FeO	MnO	MgO	CaO	Na₂O	K₂O	Total	Mg#
mafic (85-44)	40	51.12 (0.85)	0.61 (0.03)	16.58 (0.18)	7.84 (0.24)	0.059 (0.015)	10.43 (0.14)	9.28 (0.08)	2.24 (0.06)	0.39 (0.02)	98.55	70.3

Note: n = number of probe analyses. a Numbers in parentheses are the 2σ errors (standard deviation from replicate analyses) on the reported oxide wt%

of the glass starting material was inspected by electron microprobe analysis (Table 1).

Since the starting material was glassed in air we expect the starting material to have all iron as Fe^{3+} before the experiments. However, the experiments (see below for procedures) were unbuffered for f_{0_2} (oxygen fugacity). The presence of Fe-bearing olivine and orthopyroxene crystals in some of the experimental products (Table 2 and Supplemental Table S1) confirms that some of the Fe^{3+} was reduced to Fe^{2+} during the experiments. It was shown recently that increasing Fe^{3+} content of anhydrous silicate melts increases their viscosity and glass transition temperature (Di Genova et al. 2017), which indirectly means that increasing Fe^{3+} improves the quenchability. The effect of f_{0_2} on hydrous glass quenchability has not yet been studied directly. In our case we expect the Fe^{3+}/Fe^{2+} to be higher than zero, but at this time it is unconstrained.

Experimental procedures

Experiments were conducted using the ½ inch piston-cylinder apparatus (Boyd and England 1960) at the Washington University in St. Louis, Experimental Studies of Planetary Materials laboratory. We employed a single capsule, which contained an unbuffered mixture of powdered glass starting material and deionized water. We used an Au₈₀Pd₂₀ alloy capsule for all experiments. The capsule was prepared with a small lip and was fitted with a lid that was cold-welded by pressure (Avers et al. 1992). a design that has been successful in super-hydrous experiments (e.g., Brenan et al. 1994, 1995; Krawczynski et al. 2012). The lid seals when the piston load is applied to the capsule during pressurization, before heating. The capsule was surrounded by a soft-fired pyrophyllite ring. During compression, the pyrophyllite ring deformed with the capsule, which helped stop the development of shear stresses. A BaCO₃ pressure cell was used in all experiments. Most of the experiments were conducted on glass starting materials at 1 GPa, but several experiments were conducted at 1.5 GPa (see details below). Experiments were doped with different starting amounts of deionized water ranging from ~1 to ~21% of the weight of sample glass + H₂O (Table 2). Turning off the power quenched the experiments. Cooling during the finite quench duration leads to thermal contraction and a concurrent drop of pressure on the sample (Bista et al. 2015). To test whether the pressure evolution during the quench duration significantly controls the final run we quenched some of our 1 GPa experiments under isobaric (pumped pressure at quench) conditions and conducted several 1.5 GPa experiments. The maximum experimental cooling rate ranges up to 120 K/s (Fig. 2), which is common for the piston-cylinder apparatus (e.g., Zhang et al. 2017). However, the cooling rates at specific glass transition temperatures (T_g was calculated after Deubener et al. 2003) are 20–90 K/s (Fig. 2), which match those for melt inclusions that form in samples that range in particle size somewhere in between ash particles (>500 K/s) to 2 cm lapilli (up to 22 K/s; Lloyd et al. 2013; Fig. 3). Thus, the quench rates achieved in the piston-cylinder closely approximate those for the most frequent size of tephra samples used in melt inclusions studies. Each experiment used porous MgO parts to surround the sample, and experiments

were held at pressure for 5 h at 800 °C to anneal the porous MgO starting material before the temperature was increased up to maximum values (1225–1300 °C). This annealing step prevented gold from flowing into grain boundaries and pores in the MgO. Experimental durations were 16 h for 1225 °C runs and 10 h for 1300 °C runs. The run times were deemed sufficient by observing homogeneous glass as a run product in low $\rm H_2O$ experiments. Experimental conditions and run products are shown in Table 2.

Electron microprobe analysis/characterization (EPMA)

Post-quenching, several 1–2 mm pieces from each experiment were prepared for analysis and characterization by electron microprobe. Experimental products were investigated for vesiculation and quench crystallization. Quantitative measurements of the major element chemistry of quenched products were obtained using the JEOL 8200 instrument at Washington University in St. Louis. A beam current of 25 nA, an accelerating voltage of 15 kV, and a beam size of 30 µm were used for all glass analyses. EPMA analyses of experimental run products are listed in Supplemental¹ Table S1. Chemical homogeneity of the run products was checked by multiple EPMA analyses and presented in Supplemental¹ Table S1 as the standard deviation (20). Iron loss to the Au₈₀Pd₂₀ capsule was calculated by comparing the bulk glass composition to that of the starting material and shown to be always <8.5% and usually about 1–3% (Table 2).

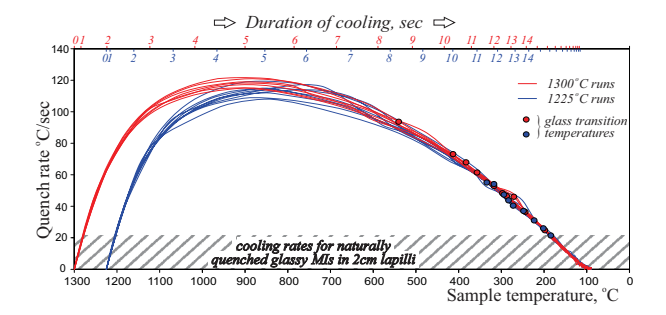


FIGURE 2. The variations of cooling rates (blue and red thin lines) during quenching of the experiments. The experimental quench rates at the glass transition temperatures (solid circles) are higher than natural cooling rates for MIs in 2 cm lapilli (gray hatching) determined by Lloyd et al. (2013). Glass transition temperatures (solid circles) are calculated for every experimental melt composition using Deubener et al. (2003).

TABLE 2. Run conditions and products for hydrous supra-liquidus experiments for 85-44 composition

Run	T (°C) P (GPa)		Pre-loaded H₂O (wt%)	Duration (h)	Phases ^a	% ΔFe ^b	T _g (°C)	
F068	1225	1.0	8.7	16	vesicular glass, quench material (96) + olivine (4)	-8.4	288	
F069	1225	1.0	12.2	16	quench material	-5.6	248	
F070	1225	1.0	15.1	16	quench material	-2.9	223	
F071	1225	1.0	18.0	14	quench material	-2.9	202	
F073	1225	1.0	8.2	16	glass + quench material	-1.2	294	
F074	1225	1.0	9.9	16	quench material	-0.6	272	
F075	1225	1.0	7.6	16	glass + quench material	0.0	304	
F076	1225	1.0	6.8	16	glass (94), quench crystals, + olivine (6)	1.9	317	
F079	1225	1.0	5.9	16	glass and rare quench crystals	-1.1	334	
F080	1225	1.0	9.0	16	vesicular glass + quench material	-0.7	283	
F083	1225	1.0	21.3	16	quench material	0.4	184	
F085	1300	1.0	1.3	10	glass (88) + pyroxene (12)	-1.4	540	
F087	1300	1.0p	3.3	10	glass	1.4	413	
F088	1300	1.0p	5.0	10	glass	8.0	357	
F089	1300	1.0p	6.8	10	glass + quench crystals	0.7	317	
F090	1300	1.0p	8.7	10	vesicular glass + quench material	3.1	288	
F091	1300	1.0p	10.0	10	quench material		271	
F097	1300	1.5	18.5	10	quench material	-3.9	198	
F098	1300	1.5	12.6	10	quench material	-2.1	244	
F099	1300	1.5	4.1	10	glass	2.4	383	
F106	1300	1.0p	8.0	10	glass + quench material	-1.6	297	
F107	1300	1.0p	12.2	10	quench material		248	

Notes: For experiments without crystals the Fe-loss was calculated via comparison of broad beam analyses (normalized to 100%) to the bulk composition. 1.0p means that pressure was maintained during quenching due to active pumping. T_g = calculated glass transition temperature based on pre-loaded H_2O content and algorithm from Deubener et al. (2003). Phase abundances in percent are given in parentheses, calculated by mass balance (Krawczynski and Olive 2011). Percent of relative Fe loss or gain from the starting material was estimated using a mass balance of the measured phase compositions and the bulk starting composition of the experiment (Krawczynski and Olive 2011).

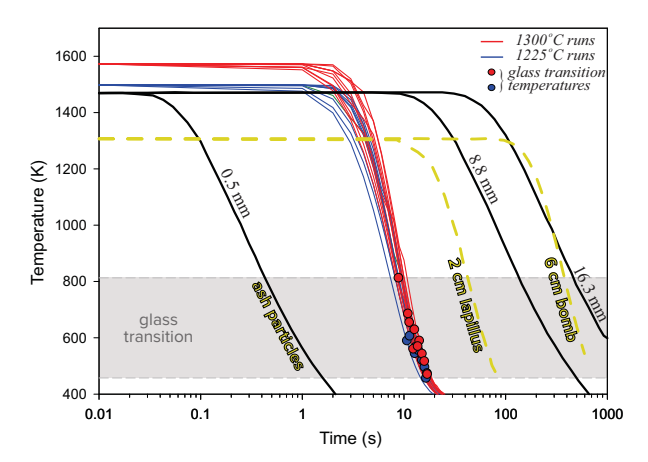


FIGURE 3. The comparison of natural and experimental temperature drop during quenching. The experimental quench rates (blue and red thin lines) are very close to cooling rates of natural glasses (black and yellow thick lines). Yellow dashed thick lines show the cooling rates of MIs in 2 cm lapilli and 6 cm vessels determined by Lloyd et al. (2013). Black thick lines are modeled cooling rates of glass in pillow lava rims at different depths from the margin reported in Cottrell and Kelley (2011). The model for the depth of 0.5 mm is assumed as a cooling rate for MIs from ash particles. The glass transition temperatures (solid circles) are determined as in Figure 2.

Imaging

Images of the experimental products presented in this study were obtained with the following instruments: an optical microscope, the JEOL 8200 electron microprobe at Washington University in St. Louis as well as a JEOL JSM-6010LA analytical scanning electron microscope and a JEOL JSM-7100F field emission scanning electron microscope housed at the University of Nevada, Reno. The images are presented in Figures 5 and 8 and also in Appendices 1 and 2.

Quantitative analysis of H2O in experimental products

To determine the dissolved H2O of our experimental run products we used a bulk extraction technique (Ihinger et al. 1994), which is based on measuring the loss on ignition of the hydrous glass. Quantification of water content was conducted using a Thermogravimetric Analyzer (TGA, Q5000IR, TA Instruments) at Washington University in St. Louis, having a sensitivity of 0.1 μg and the weighing accuracy ±0.1% (see method's details in Mielenz et al. 1953; Knowlton et al. 1981; Guggenheim and van Groos 2001; Földvári 2011). In a typical TGA analysis, 5-7 mg of sample was crushed to a fine powder in an agate mortar immediately prior to the analysis. In this way, we minimized H₂O loss from the sample, or H₂O gain by adsorption onto the powdered sample from the atmosphere. The powdered sample was placed in a platinum pan and heated at a rate of 5 °C/min to 850 °C under a flow of N2 (1 bar, 25 mL/min). Ultra-pure N2 was used for all measurements. After heating, the sample was held at 850 °C for a time (5–30 min) until no mass change greater than 1 μg per minute was observed. For each TGA run, the change in mass and temperature was recorded continuously during the entire measurement. The techniques that were employed in this study actually measure the total volatile content of experimental run products, not just the dissolved H2O. The major volatile component of the experimental run products is H2O, however other volatile species, primarily dissolved CO2, may contribute to the total volatile content. The run products from our experiments have low amounts of CO2 (~500 ppm; see details in the Results section). Such CO2 content is small compared to the H2O contents of these experiments, so that contribution to both total volatile content and H2O solubility during the quench are assumed to be negligible (e.g., Papale et al. 2006; Métrich and Wallace 2008; Shishkina et al. 2010; Steele-Macinnis et al. 2011, 2017).

H₂O determinations by TGA analyses of our experimental products also were complemented by H₂O estimations by difference from 100% totals from EPMA analysis ["volatiles by difference" (VBD) method, e.g., Nash 1992; Devine et al. 1995; King et al. 2002; Humphreys et al. 2006; Blundy and Cashman 2008]. The VBD method is widely used for quantifying the volatile contents in both experimental

(e.g., Di Carlo et al. 2006; Botcharnikov et al. 2008; Erdmann and Koepke 2016) and natural (e.g., Sommer 1977; Rutherford and Devine 1996; Métrich et al. 2004; Holtz et al. 2005) silicate glasses. The quantitative analysis of H₂O both by TGA and VBD determinations in experimental products are listed in Supplemental¹ Table S1. The estimated uncertainty for total water content using the by difference method is higher than the TGA because it takes into account the uncertainty on all the other species measured. It was shown recently that the VBD method overestimates the volatile content of hydrous glasses as much as ~1 wt% due to sub-surface charging during EPMA analysis (Hughes et al. 2019). However, the two methods agree within uncertainty for all the samples measured with both methods.

Secondary ion mass spectrometry (SIMS) analysis of volatile components

Glass chips from two experimental charges (F099, n = 3; F087, n = 3) were mounted individually in dental resin and polished on one side. After removal from the resin using acetone wash, the chips were mounted in indium metal for SIMS (secondary ion mass spectrometer) analysis. Volatile species (H2O, CO2, Cl, F, and S) and P in the experimental glasses were measured on a Cameca IMS 7f-GEO ion probe at Washington University in St. Louis. The procedure was adapted from Hauri et al. (2002) measuring monovalent anions of ¹²C, ¹⁶O, ¹H, ¹⁹F, ³⁰Si, ³¹P, ³²S, and ³⁵Cl. A primary beam (5-10 nA) accelerated to 10 kV was used to create a ~20 µm spot size. We used primary basaltic reference materials ALV-519-4-1, ALV-1833-11, ALV-1846-12, ALV-1833-1 characterized by Kumamoto et al. (2017), and Fonualei Rift:ND-60-01 (n = 10) and Mangatolu Rift:ND-70-01 (n = 11) as secondary reference materials (Lloyd et al. 2013). The primary reference glasses were used to develop calibration curves for H2O, F, P, S, and Cl. Given the high background for 12C for the standard mount, likely due to contamination derived from the standard mount, we used the secondary standards to obtain a calibration curve for CO2. A significantly lower background in ¹²C characterized the sample mount. It is noted that we report CO₂ concentrations for the experimental glasses with less confidence given that no additional secondary standard was available to confirm calculated concentrations. A synthetic pure silicate glass, Suprasil, was measured to estimate limits of detection for H2O, F, P, and S (Supplemental Table S2). CO2 is affected in the same way as mentioned above, and Cl is high in this reference glass.

Powder X-ray diffraction

The quenched products from experiments F071, F091, and F098 were ground and then analyzed using powder X-ray diffraction (XRD) to identify mineral components. All samples were mounted in zero-background Si sample holders with a 10 mm diameter well. Measurements were made on a Bruker d8 Advance diffractometer at Washington University in St. Louis, using a $\text{Cu}K\alpha$ X-ray tube and a LynxEyeXE energy-dispersive strip detector. Data were collected from 5 to 80° 20 in 0.02° steps with 0.5 s integration time; the samples were continuously rotated at 15 revolutions per minute.

RESULTS

Our results show that quenched mafic glasses, which retained the total pre-loaded $\rm H_2O$ content as dissolved $\rm H_2O$, only occurred in experimental runs with less than ~9 wt% $\rm H_2O$ (Fig. 4); at higher pre-loaded $\rm H_2O$ content (up to ~21 wt%) the experiments did not quench to a homogeneous glass. Key in this analysis is both the $\rm H_2O$ solubility in melts and the $\rm H_2O$ quenchability in glasses. At the $\rm P$ and $\rm T$ conditions of our experiments, the maximum solubility of $\rm H_2O$ in the mafic melt should be approximately 20 wt% (Mitchell et al. 2017), far exceeding observed $\rm H_2O$ contents in our quench products.

Textures of the quenched experimental run products systematically changed with increasing pre-loaded $\rm H_2O$ contents (Fig. 5). Experiments with up to 6 wt% pre-loaded $\rm H_2O$ quenched to optically clear, non-vesiculated glass. For experiments with more than 6 wt% $\rm H_2O$ but <9 wt% $\rm H_2O$, we identify a "transition zone" where run products were not completely quenched to vesicle-free glass; instead there was a mixture with areas of optically clear glass and areas of glass thoroughly permeated with quench crystals, vesicles, and devitrified glass. For our experiments with >9 wt%

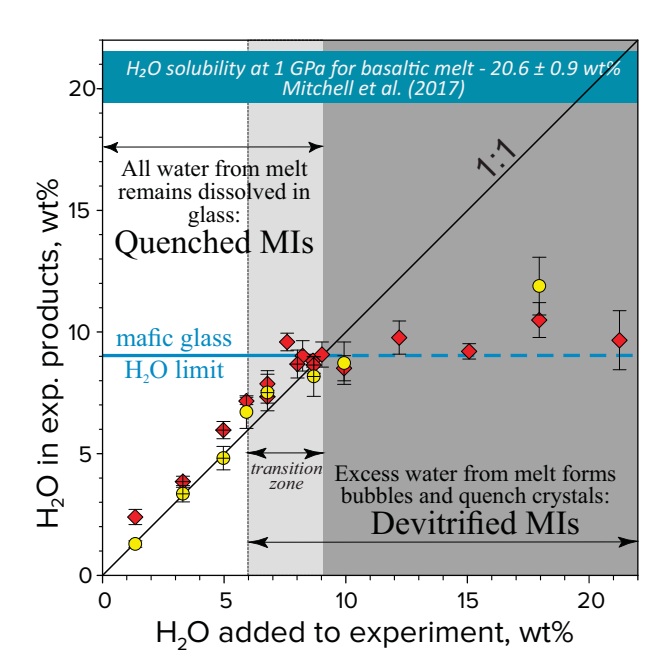


FIGURE 4. H₂O content in products of 1 GPa experiments. Red diamonds show EPMA data, yellow circles show TGA measurements (1 σ error bars). Crossed symbols are from experiments with isobaric quench. Mafic compositions have a limit for the incorporation of H₂O in the quenched glass structure, which is significantly lower than H₂O solubility at 1 GPa for basaltic melt (Mitchell et al. 2017). The blue line represents the quenchability limit for mafic compositions.

of pre-loaded H_2O , optically clear glass was not present at any amount and all experimental products were an intimate mixture of fractured, vesicular, devitrified glass, quench crystals, and hydrous products of glass alteration (see more details about textures for every sample in the Appendix¹ 1).

The quenched products from experiments F071 (18 wt% H₂O),

F091 (10 wt% H₂O), and F098 (12.6 wt% H₂O) were analyzed using powder X-ray diffraction (XRD) to identify minerals present. XRD patterns (Fig. 6) of the three run products consist of several broad and often asymmetric features on top of a background containing a broad feature near 30°. This background feature indicates a significant amorphous component, such as glass. Features in the XRD pattern at low angles (Fig. 7) are consistent with smectites (Moore and Reynolds 1997) having a range of hydration states, with apparent d-spacings spanning ~12.5 to ~14.9 Å. The identification of smectites is further supported by the presence of asymmetric features near 19 and 34° (Fig. 6), which are (hk0) bands indicative of a turbostratically stacked phyllosilicate. A phyllosilicate (060) feature present near 60° consists of a composite peak (Fig. 7) corresponding to two or more phases with d-spacings in the range of 1.530 to 1.542 Å, indicating all phases are trioctahedral in nature (Moore and Reynolds 1997). Additional features present in all patterns (Fig. 6) likely originate from higher-order basal reflections associated with smectites having different degrees of hydration and additional turbostratic (hk0) bands. However, some features present may also result from partial interstratification with other phyllosilicates. In addition to the above features, sample F098 contains sharp diffraction peaks near 5.9, 11.8, and 17.8° (Figs. 6 and 7) corresponding to the (001), (002), and (003) reflections, respectively, of chlorite. The narrow features at higher angles that are unique to this sample also likely originate from chlorite, although additional accessory crystalline phases may be present as well. While samples F098 and F071 contain two peaks from periclase, this phase is a contaminant originating from the experimental matrix outside of the reaction capsule. High-quality SEM images of those three non-glassy experimental products with comparison to a glassy one (experiment F099) are presented in Figure 8 (more SEM images of those experiments can be found in Appendix¹ 2). The SEM images visually confirm the presence of vast non-glassy material with a flaky appearance (Figs. 8a, 8b, and 8c). The samples' apparent flakiness cannot be easily confused with the appearance of blocky, conchoidally fractured glass (Fig. 8d).

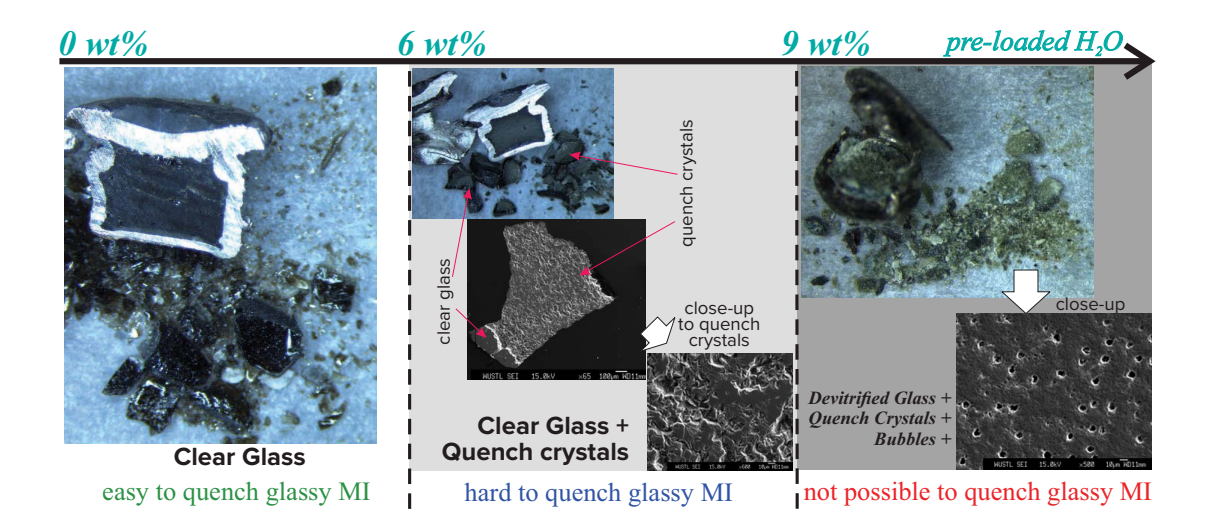


FIGURE 5. Texture changing with increasing pre-loaded H_2O contents. The amount of preloaded H_2O increases from left to right, in wt%. See text for discussion.

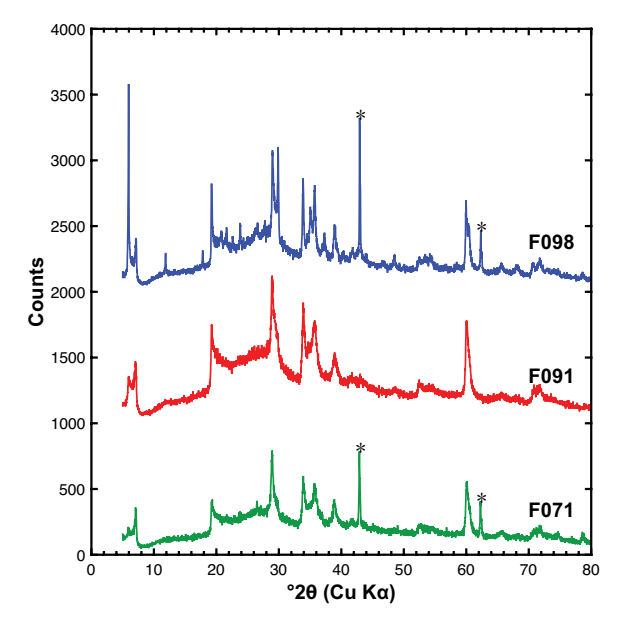


FIGURE 6. Powder XRD patterns of products from the three experiments. Asterisks (*) indicate a periclase (MgO) contaminant from the experimental assembly. Patterns F091 and F098 have been offset vertically for clarity.

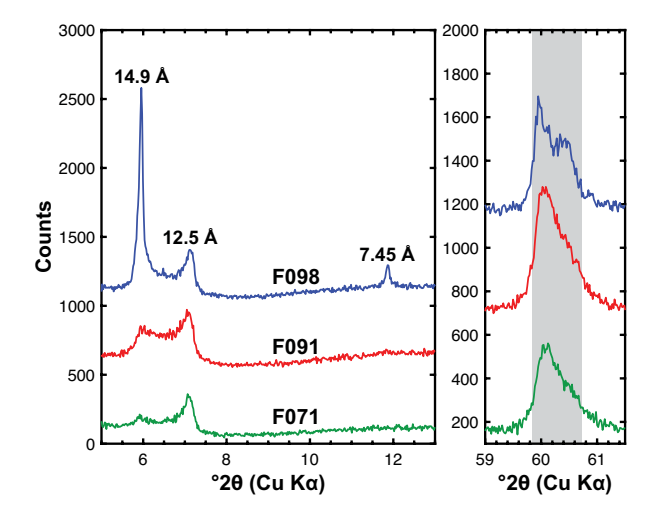


FIGURE 7. (**left**) Low-angle region of powder XRD patterns of the experimental products, highlighting phyllosilicate basal reflections. (**right**) Phyllosilicate (060) features, with the gray band indicating a *d*-spacing range of 1.525 to 1.545 Å. Patterns F091 and F098 have been offset vertically for clarity.

Basaltic hydrated experimental glasses F099 and F087 were analyzed by SIMS and concentrations are reported in Supplemental Table S2. SIMS results agree well with how much water was initially loaded into the capsules and with other determinations of water contents after the experiment. CO₂ contents determined by SIMS (note that concentrations are reported with less confidence) are 461 ppm (F087) and 575 ppm (F099), which suggests that CO₂ did not contribute significantly to any weight loss determined by TGA. The same applies for the other volatile elements that never exceed 200 ppm.

DISCUSSION

Solubility vs. quenchability

The glass transition—a conversion from a liquid silicate melt to a solid glass—is an important process responsible for quenching glassy MIs, both in natural systems and experimentally. This kinetic process strongly depends on parameters such as melt polymerization and cooling rates (Dingwell and Webb 1990). The temperature of the glass transition (T_g) is also controlled by the amount of dissolved H₂O, which de-polymerizes a melt (e.g., Mysen 2014). While T_g of natural maffe dry melts is about 1000 K, $T_{\rm g}$ for hydrous melts is significantly lower; as low as 450 K for a melt with 20 wt% of dissolved H₂O (Deubener et al. 2003). For higher melt H₂O contents, the lower T_g requires particularly high cooling rates to quench a melt to a glass. During the quenching process, the cooling rate varies (Fig. 2) and is typically highest as quenching commences at high temperatures. Thus, melts with no or low dissolved H₂O content quench easily as the glass transition temperature is rapidly reached. In contrast, melts with a low T_{\circ} (for example, H₂O-rich melts) require high peak cooling rates at high temperatures, which would be sustained to low temperatures (Fig. 2).

Under normal quenching conditions for piston-cylinder experiments, the quenching is achieved by shutting off power to the device. This instantaneous loss of power cools the experiment at rates (Figs. 2 and 3) similar to natural erupted samples (Lloyd et al. 2013). This cooling leads to thermal contraction and a concurrent drop of pressure on the sample (Bista et al. 2015). Such pressure change may affect the run products if the sample becomes wateroversaturated prior to reaching $T_{\rm g}$ as a consequence of the pressure drop in the sample. In our experiments, we tracked the pressure change at quench in every experiment (Fig. 9). The glass transition is reached in all experiments at pressures higher than 500 MPa. Two steps were taken to test whether the pressure evolution in our experiments controls the quenchability of the sample: (1) some of our 1 GPa experiments (Table 2; Fig. 9) were quenched under isobaric (without pressure drop) conditions and (2) several 1.5 GPa experiments were conducted (see Table 2 and Fig. 9). The latter higher pressure experiments had a contraction pressure drop, but still maintained pressures over 900 MPa. All experiments, including those with the modified run procedures, ended up with the same experimental results. In all cases, our observed limit of ~9 wt% dissolved H₂O in the experimental glass is much lower than the H₂O content in the melt suggested from solubility experiments that determined the H₂O solubility indirectly through partitioning into olivine (Mitchell et al. 2017). Thus, our experiments indicate that the melt to glass transition fundamentally effects how much water can remain dissolved in glass. The release of water from the melt occurred because of the structural change related to the meltglass transition and it was not in response to lower H₂O solubility limits at lower pressures.

How $\rm H_2O$ is accommodated in the atomic structure of the glass may change during the melt-glass transition, likely due to changes in the speciation of hydrogen. In melts, water dissolves as both hydroxyl groups (OH⁻) and molecular water ($\rm H_2O_m$) (Stolper 1982a, 1982b; Silver and Stolper 1989; McMillan 1994). The incorporation of hydroxyl groups is well understood. Hydroxyl groups are thought to break bridging oxygen bonds and therefore

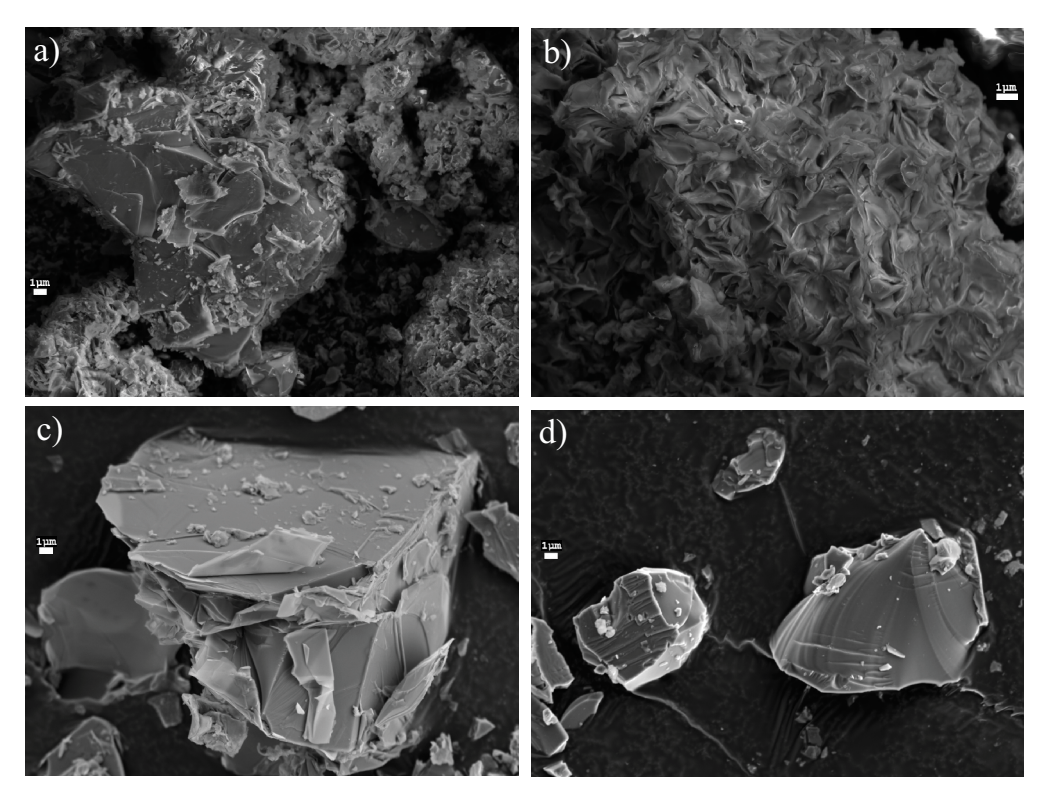


FIGURE 8. SEM images of the non-glassy run products. (a) F071, (b) F091, (c) F098, mainly consisting of phyllosilicates (having flaky appearance)—in comparison with the glassy one (d) F099.

are easily structurally bound within the silicate melt (e.g., Mysen 2014). The structural position of molecular water in silicate melt is less clear. As a neutral, although polar species, molecular water potentially behaves similarly to noble gases, which fit into holes in the melt/glass structure (Carroll and Stolper 1993; Guillot and

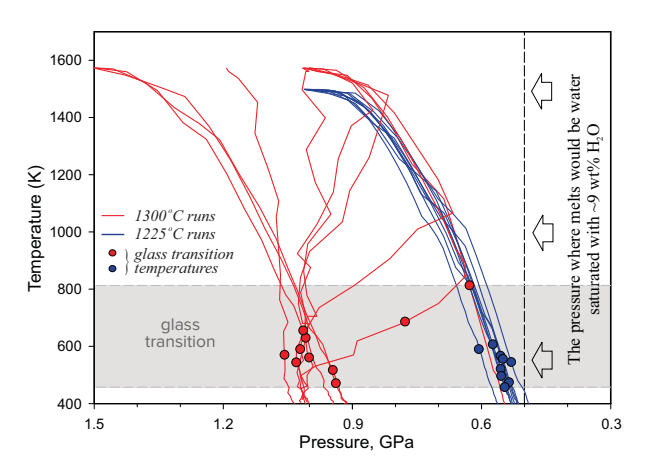


FIGURE 9. Pressure-drop during the quenching period of hydrous experiments at 1 and 1.5 GPa. The pressure for each experiment at the point when it crossed the estimated glass transition temperature was always at least 50-100 MPa above 0.5 GPa which is where ~ 9 wt% would be the $\rm H_2O$ solubility in a basaltic melt (e.g., Shishkina et al. 2010, 2012, and references within). The glass transition temperatures (solid circles) are determined as in Figure 2.

Sarda 2006; Guillot and Sator 2012). If water occupies free volumes or structural cavities in the melt (Paonita 2005), the so-called ionic porosity (i.e., the volume of holes in the structure; Carroll and Stolper 1993) may control the solubility of water molecules in silicate melt/glass. Compared to high temperature and higher H₂O_{total} contents where water is primarily incorporated as hydroxyl groups (OH⁻) into the silicate melt structure (Nowak and Behrens 1995; Chertkova and Yamashita 2015), OH- groups convert to molecular water during cooling and quenching to a glass (Stolper 1982a, 1982b; Silver and Stolper 1989). The ratio of hydrogen bound as hydroxyl groups to molecular water (OH-/H₂O_m) decreases from up to 4 in the melt to 0.25 in quenched glass (for an experimental charge with 8 wt% of H₂O_{total}; Chertkova and Yamashita 2015). The drastic increase in the amount of molecular H₂O during quenching may exceed the ability of the glass to accommodate water in its structural cavities. For hydrous arc magmas with 14-20 wt% of H₂O_{total} (36–46 mol% of H₂O), quenching to glass in MIs might result in occupying all free structural cavities by molecular H₂O and exsolving excess H₂O to a fluid or gas phase (bubbles), which can promote alteration/devitrification (Anderson 1991) through crystallization of hydrous minerals and/or over-pressurize the inclusion causing the host crystal to rupture.

P-T paths of experimental products at quench vs. natural MIs

When a melt inclusion forms in nature, the pressure inside and outside the olivine is equal. During magma ascent and eruption, the pressure inside the melt inclusion will be reduced due to a combination of several factors, such as elastic deformation of the host mineral, post entrapment crystallization, diffusive volatile components loss, and volume change at the glass transition. The pressure inside the melt inclusion is reduced, but is ultimately greater than zero (e.g., Steele-MacInnis et al. 2011; Gaetani et al. 2012; Hartley et al. 2014; Moore et al. 2015; Wallace et al. 2015a; Steele-MacInnis et al. 2017). Some of the contributions to the pressure drop might be minimized in the case of rapid magmatic ascent, but overall partial decompression will occur. The pressure drop in a MI can be calculated (Zhang 1998), and is about 3-4 kbar for olivine-hosted MIs that are <150 µm in size and are formed at a depth of 20–30 km (e.g., Schiano and Bourdon 1999; Maclennan 2017). This pressure drop is similar in magnitude to the pressure change resulting from thermal contraction during the quenching of our experiments under uncontrolled pressure conditions (described above) (Fig. 9). Moreover, even the experiments with isobaric quench produced the same run products as the experiments with a pressure drop. Thus, our experiments represent a conservative estimate for the maximum water content that can quench to glass in natural melt inclusions, and we suggest that decompression conditions at quench in our experiments were comparable to natural MIs.

MI re-equilibration vs. quenchability

It is often interpreted that the most water-rich melt inclusions analyzed for a given volcanic suite of samples experienced the least water loss due to diffusive re-equilibration, and thus are the best estimates for the highest water contents of primitive arc magmas (e.g., Métrich and Wallace 2008; Bouvet de Maisonneuve et al. 2012; Lloyd et al. 2013 and references therein). This is fundamentally different than what we are showing in this study, which is that there is a physical limit to how much water a glassy melt inclusion can hold. Because the highest values of measured dissolved H₂O in melt inclusions coincide with the experimentally determined quenching limit, it precludes the use of the melt inclusion record to determine the existence and/or prevalence of super-hydrous arc magmas. Indeed, MIs lose significant amounts of water during the slow ascent of arc magma to the surface due to rapid hydrogen diffusion. But even in cases when magma ascends extremely rapidly and keeps most of its original H₂O content, a MI with high water content (>9 wt%) is unlikely to be quenched to a glassy MI.

Deep-formed crystals are brought to the surface in arcs fairly commonly. Mantle xenoliths, while not extremely abundant, are ubiquitous among most arcs (e.g., Bryant et al. 2007; Ionov 2010), and are much larger in size than single crystals. If xenoliths can make it to the surface from the mantle, certainly deep-formed crystals can as well. In the case of arcs there is also a common occurrence of primitive olivine and pyroxene phenocrysts (Mg#≈ 90 and more; e.g., Nye and Reid 1986; Ozerov 2000; Straub et al. 2008; Ruprecht and Plank 2013; Gavrilenko et al. 2016a, 2016b; Streck and Leeman 2018), which are the very first crystals to form from melts in equilibrium with the mantle, and are most likely formed at depth. Many of those deep primitive crystals contain MIs (e.g., Sobolev and Chaussidon 1996; Kamenetsky et al. 1997; Kamenetsky et al. 2002; Churikova et al. 2007; Portnyagin et al. 2007; Johnson et al. 2008; Cooper et al. 2010; Mironov and Portnyagin 2011; Ruscitto et al. 2011; Tolstykh et al. 2012; Mironov et al. 2015; Walowski 2015) with a range in volatile contents.

What then can explain the lack of high-pressure glassy melt inclusions? There are two non-mutually exclusive mechanisms for this: re-equilibration of hydrogen at shallow pressures and the existence of super-hydrous melt inclusions that cannot quench to a glass. For melt inclusions to retain >9 wt% H₂O until eruption and quenching, they must ascend rapidly to the surface from depths where water solubility exceeds 9 wt%. Such rapid ascent has been proposed for some arc volcanoes (Gordeychik et al. 2018). We would still emphasize that H₂O re-equilibration between MIs and matrix melt is known to be fast and likely controls the final recorded H₂O content in MIs. Partial to complete re-equilibration occurs on timescales of hours to days (e.g., Qin et al. 1992; Gaetani et al. 2012; Bucholz et al. 2013) depending on the crystal and melt inclusion size, the magma temperature, and the ascent rate. However, as diffusive flux out of the melt inclusions is a direct function of the concentration gradient between the matrix melt and the melt inclusion, re-equilibration is most effective at shallow pressures, where fast ascent on the order of minutes to hours has been suggested (e.g., Demouchy et al. 2006; Humphreys et al. 2008; Lloyd et al. 2014; Ferguson et al. 2016; Zellmer et al. 2016; Petrelli et al. 2018 and references therein). In the lower crust where H₂O solubility is high the gradient of H₂O contents between a MI and surrounding magma is small and re-equilibration is slowed. Thus, ascent driven water loss from melt inclusions below 10–12 wt% H₂O is limited until mid-crustal depth (6-7 kbar for 10-12 wt% H₂O; Shishkina et al. 2010). Rapid magma ascent is likely in some cases due to such factors as extreme buoyancy of hydrous magmas (e.g., Herzberg et al. 1983; Ochs and Lange 1999), the rapid dynamics of dike propagation (Rubin 1993; Dahm 2000; Taisne and Jaupart 2011; Rivalta et al. 2015), and absence of a crustal magma chamber for an arc volcano (Ariskin et al. 1995; Ozerov et al. 1997; Lees et al. 2007; Ozerov 2009; Mironov and Portnyagin 2011; Kayzar et al. 2014; Levin et al. 2014), which could help to preserve near-original H₂O contents in primitive melt inclusions (and avoid/minimize rapid re-equilibration of a MI with external magma).

Comparison of experimental results to natural MIs

Most mafic MIs from subduction zone settings have low H₂O content (<4 wt%; Fig. 1) presumably caused by extensive degassing and diffusive equilibration through olivine-host crystals. The emphasis in recent studies has shifted to analyzing melt inclusions from fast cooled olivine grains in tephra particles, which often show H₂O content of >4 wt% (e.g., Johnson et al. 2008), but do not exceed 8.5 wt% of H₂O (de Moor et al. 2013). The maxima in dissolved H₂O found in quickly cooled olivine crystals (Fig. 1) are normally interpreted to represent the maximum H₂O content of arc magmas (e.g., Plank et al. 2013). Our experiments provide an alternative interpretation of natural glassy MI; that this maximum content observed in nature represents a physicochemical limit to the amount of H₂O that can be found dissolved in a glassy melt inclusion.

Studies that focus on measuring water contents of glassy melt inclusions show that MI measurements are most abundant in the range of 1 to 6 wt% H₂O contents (99% of the data points). Finding glassy melt inclusions in this range is common and consistent with our experiments. More hydrous glassy melt inclusions become increasingly rare in what we refer to in the experiments as the

"transition zone" (6–9 wt% H₂O, Fig. 1). For the experiments, we propose that quenching to an optically clear single-phase glass is kinetically controlled and by analogy we expect natural MIs that form from melts with 6–9 wt% of H₂O to quench to non-glassy inclusions. Only in the rare cases where quench rates are extremely high and samples experience natural kinetic barriers to forming quench crystals (i.e., little undercooling before the glass transition is achieved) can glassy melt inclusions form. The rarity of glassy melt inclusions with high water contents is thus not directly tied to the rarity of high water content melts but to the preferential analysis of glassy melt inclusions that get selected for study. Berndt et al. (2002) were able to quench an optically clear (bubble- and crystalfree) glass from a basaltic melt containing 9.38 wt% of H₂O using a rapid-quench device in an internally heated pressure vessel for quench rates of approximately ~150 K/s. The higher cooling rate at $T_{\rm g}$ is the likely reason why Berndt et al. (2002) obtained better quality quenched glass than ones from our study. Indeed, this result (9.38 wt% of H₂O) is the maximum for published experiments on mafic quenched glasses and is still consistent with our results. However, it is probably not possible to obtain such high cooling rates (\sim 150 K/s) at T_g in natural MIs.

For our experiments with >9 wt% of loaded $\rm H_2O$, optically clear glass was not present and instead an intimate mixture of fractured, vesicular, devitrified glass, quench crystals, and hydrous products of glass alteration comprised all experimental products. X-ray diffraction measurements on experimental run products from super-hydrous experiments show mineralogy of run products that includes low-temperature hydrous minerals (smectites, chlorite) and amorphous material that is likely poorly quenched melt. A similar mineralogy has been described in devitrified MIs in olivine (e.g., Imae and Ikeda 2007).

There are multiple possible devitrification mechanisms, which cannot be distinguished with our current experimental setup: (1) during the quench, water exsolves and alters the glass in the experiment producing a palagonite-like substance (Bonatti 1965), which is basically a mixture of various smectites and potentially zeolites and oxides (Stroncik and Schmincke 2002); (2) a devitrification mechanism where the crystallization temperature of hydrous minerals is higher than the $T_{\rm g}$, which leads to the nucleation and crystallization of hydrous minerals before a glass transition. More detailed documentation of the devitrification mechanism would require in-situ observations. Nevertheless, natural melt inclusions with H₂O contents above 9 wt% most likely never quench to a glass, and form devitrified inclusions (Skirius et al. 1990; Anderson 1991; Imae and Ikeda 2007) or exsolve water that may overpressurize the inclusion and break the host crystal (decrepitation, e.g., Wanamaker et al. 1990).

Our results indicate that 9 wt% of dissolved H₂O is a physical limit for silicate mafic melts to quench to a homogeneous glass under naturally occurring cooling rates (Fig. 4). Thus, the observed maximum of 8–9 wt% H₂O from glassy mafic MI studies may correspond to a quenchability limit (Fig. 1). We speculate that melt inclusions of H₂O-rich magmas (>9 wt% H₂O) may exist, but they may never get preserved as glassy MIs. Therefore, studies that focus solely on glassy single-phase MIs in olivine (or any mineral host) will systematically be limited to finding dissolved water contents <8–9 wt% and therefore may not fully characterize the magmatic H₂O budget in subduction zones.

IMPLICATIONS

Our hydrothermal experiments show that the maxima of 8–9 wt% of dissolved $\rm H_2O$ from melt inclusions (MIs) studies match the physicochemical limit of quenched glassy-melt inclusions. At higher dissolved $\rm H_2O$ contents and natural quenching rates mafic melts cannot form glassy MIs. The possibility that such a limit for glassy MIs exists has never before been directly studied experimentally and requires a reevaluation of using MIs as a primary tool to estimate global water fluxes at arcs. MIs likely form at all depths where crystallization occurs, and the lack of deeply formed and equilibrated MIs in the existing literature suggests there might be a higher probability for super-hydrous (>9 wt% of $\rm H_2O$) magmas than previously recognized. The results of this study have identified five main closing thoughts:

- Glassy MIs are excellent recorders of pre-eruptive H₂O contents in the uppermost part of the crust, where the solubility limit for hydrous magmas is ≤6–7 wt% H₂O. Thus, MI studies focusing on degassing and eruption-style phenomena are not affected by our results.
- A higher abundance of magmas containing >10 wt% of H₂O may explain why dense primitive magmas in convergent margins can quickly reach the surface without much crystallization and fractionation (Herzberg et al. 1983; Kohn et al. 1989; Ruprecht and Plank 2013) despite a low-density filter in the form of evolved magmas and crust in their path.
- Because glass quenchability depends on the amount of water in a mafic sample, MI studies that focus on single-phase glassy MIs are introducing a previously unrecognized sampling bias into our understanding of primitive magmas.
- Our findings suggest that examining the mineralogy of nonglassy melt inclusions found in quickly cooled environments such as small lapilli or even ash deposits for the presence of chlorites or smectites may be used to identify super-hydrous magmas.
- Estimates of total water contents returned to the crust/ atmosphere by tectonic recycling based on studies of MIs (e.g., Straub and Layne 2003; Wallace 2005; Parai and Mukhopadhyay 2012; Wallace et al. 2015b; Peslier et al. 2017) likely underestimate the amount of returned H₂O. Recent geophysical studies (Cai et al. 2018) also see evidence for more extensive hydration of incoming slabs at arcs, which support the idea more H₂O is getting returned to the surface through subduction zones than previously recognized.

FUNDING

M.G. acknowledges support from McDonnell Center for the Space Sciences. M.K. acknowledges support from U.S. National Science Foundation grant EAR 1654683. P.R. acknowledges support from U.S. National Science Foundation grant EAR 1719687. J.G.C. acknowledges support from U.S. National Aeronautics and Space Administration grant NNX14AJ95G.

ACKNOWLEDGMENTS

We thank Paul Carpenter for invaluable assistance with EPMA analyses at Washington University in St. Louis. Additionally we are grateful to Tatiana Shishkina for thorough discussion and to Hélène Couvy for her comprehensive assistance in lab work. We thank Terry Plank for providing secondary SIMS standards ND-60-01 and ND70-01. Maxim Portnyagin, Glenn Gaetani, Adam Kent, Thomas Sisson, and Michel Pichavant are sincerely thanked for providing insightful comments and criticism that helped us to rethink some of our ideas and sharpened the discussion of the paper. Constructive reviews from Matthew Steele-MacInnis, Michael Rowe, and one anonymous reviewer improved the clarity of our arguments and data presentation. We thank Kyle Ashley for his editorial handling of the manuscript.

REFERENCES CITED

- Anderson, A.T. (1991) Hourglass inclusions: Theory and application to the Bishop Rhyolitic Tuff. American Mineralogist, 76, 530–547.
- Ariskin, A.A., Barmina, G.S., Ozerov, A.Y., and Nielsen, R.L. (1995) Genesis of highalumina basalts from Klyuchevskoi volcano. Petrology, 3(5), 449–472.
- Auer, S., Bindeman, I., Wallace, P., Ponomareva, V., and Portnyagin, M. (2009) The origin of hydrous, high-δi⁸O voluminous volcanism: diverse oxygen isotope values and high magmatic water contents within the volcanic record of Klyuchevskoy volcano, Kamchatka, Russia. Contributions to Mineralogy and Petrology, 157(2), 209–230. DOI: 10.1007/s00410-008-0330-0
- Ayers, J.C., Brenan, J.B., Watson, E.B., Wark, D.A., and Minarik, W.G. (1992) A new capsule technique for hydrothermal experiments using the piston-cylinder apparatus. American Mineralogist, 77, 1080–1086.
- Baker, D.R., and Alletti, M. (2012) Fluid saturation and volatile partitioning between melts and hydrous fluids in crustal magmatic systems: The contribution of experimental measurements and solubility models. Earth-Science Reviews, 114(3-4), 298–324. DOI: 10.1016/j.earscirev.2012.06.005
- Baker, M.B., Grove, T.L., and Price, R. (1994) Primitive basalts and andesites from the Mt. Shasta region, N. California: products of varying melt fraction and water content. Contributions to Mineralogy and Petrology, 118(2), 111–129. DOI: 10.1007/bf01052863
- Behrens, H., Misiti, V., Freda, C., Vetere, F., Botcharnikov, R.E., and Scarlato, P. (2009) Solubility of H₂O and CO₂ in ultrapotassic melts at 1200 and 1250 °C and pressure from 50 to 500 MPa. American Mineralogist, 94, 105–120. DOI: 10.2138/am.2009.2796
- Berndt, J., Liebske, C., Holtz, F., Freise, M., Nowak, M., Ziegenbein, D., Hurkuck, W., and Koepke, J. (2002) A combined rapid-quench and H₂-membrane setup for internally heated pressure vessels: Description and application for water solubility in basaltic melts. American Mineralogist, 87, 1717–1726. DOI: 10.2138/am-2002-11-1222
- Bista, S., Stebbins, J.F., Hankins, W.B., and Sisson, T.W. (2015) Aluminosilicate melts and glasses at 1 to 3 GPa: Temperature and pressure effects on recovered structural and density changes. American Mineralogist, 100, 2298–2307. DOI: 10.2138/ am-2015-5258
- Blundy, J., and Cashman, K. (2008) Petrologic reconstruction of magmatic system variables and processes. Reviews in Mineralogy and Geochemistry, 69, 179–239. Bonatti, E. (1965) Palagonite, hyaloclastites and alteration of volcanic glass in the ocean.
- Bulletin Volcanologique, 28(1), 257–269. DOI: 10.1007/bf02596930
- Botcharnikov, R.E., Almeev, R.R., Koepke, J., and Holtz, F. (2008) Phase relations and liquid lines of descent in hydrous ferrobasalt—Implications for the Skaergaard Intrusion and Columbia River Flood Basalts. Journal of Petrology, 49(9), 1687–1727. DOI: 10.1093/petrology/egn043
- Bouvet de Maisonneuve, C., Dungan, M.A., Bachmann, O., and Burgisser, A. (2012) Insights into shallow magma storage and crystallization at Volcán Llaima (Andean Southern Volcanic Zone, Chile). Journal of Volcanology and Geothermal Research, 211-212, 76–91. DOI: 10.1016/j.jvolgeores.2011.09.010
- Boyd, F.R., and England, J.L. (1960) Apparatus for phase-equilibrium measurements at pressures up to 50 kilobars and temperatures up to 1750°C. Journal of Geophysical Research, 65(2), 741–748. DOI: 10.1029/JZ065i002p00741
- Brenan, J.M., Shaw, H.F., Phinney, D.L., and Ryerson, F.J. (1994) Rutile-aqueous fluid partitioning of Nb, Ta, Hf, Zr, U and Th: implications for high field strength element depletions in island-arc basalts. Earth and Planetary Science Letters, 128(3), 327–339. DOI: 10.1016/0012-821X(94)90154-6
- Brenan, J.M., Shaw, H.F., Ryerson, F.J., and Phinney, D.L. (1995) Mineral-aqueous fluid partitioning of trace elements at 900°C and 2.0 GPa: Constraints on the trace element chemistry of mantle and deep crustal fluids. Geochimica et Cosmochimica Acta, 59(16), 3331–3350. DOI: 10.1016/0016-7037(95)00215-L
- Bryant, J.A., Yogodzinski, G.M., and Churikova, T.G. (2007) Melt-mantle interactions beneath the Kamchatka arc: Evidence from ultramafic xenoliths from Shiveluch volcano. Geochemistry, Geophysics, Geosystems, 8(4), Q04007. DOI: 10.1029/2006ge001443
- Bucholz, C.E., Gaetani, G.A., Behn, M.D., and Shimizu, N. (2013) Post-entrapment modification of volatiles and oxygen fugacity in olivine-hosted melt inclusions. Earth and Planetary Science Letters, 374, 145–155. DOI:10.1016/j.epsl.2013.05.033.
- Cai, C., Wiens, D.A., Shen, W., and Eimer, M. (2018) Water input into the Mariana subduction zone estimated from ocean-bottom seismic data. Nature, 563, 389–392.
- Carmichael, I.S. (2002) The andesite aqueduct: perspectives on the evolution of intermediate magmatism in west-central (105–99°W) Mexico. Contributions to Mineralogy and Petrology, 143(6), 641–663. DOI: 10.1007/s00410-002-0370-9
- Carroll, M.R., and Stolper, E.M. (1993) Noble gas solubilities in silicate melts and glasses: New experimental results for argon and the relationship between solubility and ionic porosity. Geochimica et Cosmochimica Acta, 57(23), 5039–5051. DOI: 10.1016/0016-7037(93)90606-W
- Cashman, K.V. (2004) Volatile controls on magma ascent and eruption. In R.S.J. Sparks and C.J. Hawkesworth, Eds., The State of the Planet: Frontiers and Challenges in Geophysics, 150, p. 109–124. American Geophysical Union.
- Chen, Y., Provost, A., Schiano, P., and Cluzel, N. (2011) The rate of water loss from olivine-hosted melt inclusions. Contributions to Mineralogy and Petrology, 162(3), 625–636. DOI: 10.1007/s00410-011-0616-5

- Chertkova, N., and Yamashita, S. (2015) In situ spectroscopic study of water speciation in the depolymerized Na₂Si₂O₅ melt. Chemical Geology, 409, 149–156. DOI: 10.1016/j.chemgeo.2015.05.012
- Churikova, T., Wörner, G., Mironov, N., and Kronz, A. (2007) Volatile (S, Cl and F) and fluid mobile trace element compositions in melt inclusions: implications for variable fluid sources across the Kamchatka arc. Contributions to Mineralogy and Petrology, 154(2), 217–239. DOI: 10.1007/s00410-007-0190-z
- Cooper, L.B., Plank, T., Arculus, R.J., Hauri, E.H., Hall, P.S., and Parman, S.W. (2010) High-Ca boninites from the active Tonga Arc. Journal of Geophysical Research: Solid Earth, 115(B10), B10206. DOI: 10.1029/2009JB006367
- Cottrell, E., and Kelley, K.A. (2011) The oxidation state of Fe in MORB glasses and the oxygen fugacity of the upper mantle. Earth and Planetary Science Letters, 305(3–4), 270–282. DOI: 10.1016/j.epsl.2011.03.014
- Dahm, T. (2000) On the shape and velocity of fluid-filled fractures in the Earth. Geophysical Journal International, 142(1), 181–192. DOI: 10.1046/j.1365-246x.2000.00148.x
- Danyushevsky, L.V., McNeill, A.W., and Sobolev, A.V. (2002) Experimental and petrological studies of melt inclusions in phenocrysts from mantle-derived magmas: an overview of techniques, advantages and complications. Chemical Geology, 183(1–4), 5–24. DOI: 10.1016/S0009-2541(01)00369-2
- de Moor, J.M., Fischer, T.P., King, P.L., Botcharnikov, R.E., Hervig, R.L., Hilton, D.R., Barry, P.H., Mangasini, F., and Ramirez, C. (2013) Volatile-rich silicate melts from Oldoinyo Lengai volcano (Tanzania): Implications for carbonatite genesis and eruptive behavior. Earth and Planetary Science Letters, 361, 379–390. DOI: 10.1016/j.epsl.2012.11.006
- Demouchy, S., Jacobsen, S.D., Gaillard, F., and Stern, C.R. (2006) Rapid magma ascent recorded by water diffusion profiles in mantle olivine. Geology, 34(6), 429–432.
- Deubener, J., Müller, R., Behrens, H., and Heide, G. (2003) Water and the glass transition temperature of silicate melts. Journal of Non-Crystalline Solids, 330(1), 268–273. DOI: 10.1016/S0022-3093(03)00472-1
- Devine, J.D., Gardner, J.E., Brack, H.P., Layne, G.D., and Rutherford, M.J. (1995) Comparison of microanalytical methods for estimating H₂O contents of silicic volcanic glasses. American Mineralogist, 80, 319–328. DOI: 10.2138/am-1995-3-413
- Di Carlo, I.D.A., Pichavant, M., Rotolo, S.G., and Scaillet, B. (2006) Experimental Crystallization of a High-K Arc Basalt: the Golden Pumice, Stromboli Volcano (Italy). Journal of Petrology, 47(7), 1317–1343. DOI: 10.1093/petrology/egl011
- Di Genova, D., Vasseur, J., Hess, K.-U., Neuville, D.R., and Dingwell, D.B. (2017) Effect of oxygen fugacity on the glass transition, viscosity and structure of silica- and iron-rich magmatic melts. Journal of Non-Crystalline Solids, 470, 78–85.
- Dingwell, D.B., and Webb, S.L. (1990) Relaxation in silicate melts. European Journal of Mineralogy, 2(4), 427–449. DOI: 10.1127/ejm/2/4/0427
- Erdmann, M., and Koepke, J. (2016) Silica-rich lavas in the oceanic crust: experimental evidence for fractional crystallization under low water activity. Contributions to Mineralogy and Petrology, 171(10), 83. DOI: 10.1007/s00410-016-1294-0
- Esposito, R., Lamadrid, H.M., Redi, D., Steele-MacInnis, M., Bodnar, R.J., Manning, C.E., De Vivo, B., Cannatelli, C., and Lima, A. (2016) Detection of liquid H₂0 in vapor bubbles in reheated melt inclusions: Implications for magmatic fluid composition and volatile budgets of magmas? American Mineralogist, 101, 1691–1695.
- Ferguson, D.J., Gonnermann, H.M., Ruprecht, P., Plank, T., Hauri, E.H., Houghton, B.F., and Swanson, D.A. (2016) Magma decompression rates during explosive eruptions of Kīlauea volcano, Hawaii, recorded by melt embayments. Bulletin of Volcanology, 78(10), 1–12. DOI: 10.1007/s00445-016-1064-x
- Fischer, T.P., and Marty, B. (2005) Volatile abundances in the sub-arc mantle: insights from volcanic and hydrothermal gas discharges. Journal of Volcanology and Geothermal Research, 140(1–3), 205–216. DOI: 10.1016/j.jvolgeores.2004.07.022.
- Földvári, M. (2011) Handbook of Thermogravimetric System of Minerals and Its Use in Geological Practice, 179 p. Geological Institute of Hungary (=Magyar Állami Földtani Intézet).
- Frezzotti, M.-L. (2001) Silicate-melt inclusions in magmatic rocks: applications to petrology. Lithos, 55(1), 273–299. DOI: 10.1016/S0024-4937(00)00048-7
- Gaetani, G.A., and Watson, E.B. (2000) Open system behavior of olivine-hosted melt inclusions. Earth and Planetary Science Letters, 183(1–2), 27–41. DOI: 10.1016/ S0012-821X(00)00260-0
- Gaetani, G.A., O'Leary, J.A., Shimizu, N., Bucholz, C.E., and Newville, M. (2012) Rapid reequilibration of H₂O and oxygen fugacity in olivine-hosted melt inclusions. Geology, 40(10), 915–918. DOI: 10.1130/g32992.1
- Gavrilenko, M., Herzberg, C., Vidito, C., Carr, M.J., Tenner, T., and Ozerov, A. (2016a) A calcium-in-olivine geohygrometer and its application to subduction zone magmatism. Journal of Petrology, 57(9), 1811–1832. DOI: 10.1093/petrology/egw062
- Gavrilenko, M., Ozerov, A., Kyle, P.R., Carr, M.J., Nikulin, A., Vidito, C., and Danyushevsky, L. (2016b) Abrupt transition from fractional crystallization to magma mixing at Gorely volcano (Kamchatka) after caldera collapse. Bulletin of Volcanology, 78, 47. DOI: 10.1007/s00445-016-1038-z
- Gordeychik, B., Churikova, T., Kronz, A., Sundermeyer, C., Simakin, A., and Wörner, G. (2018) Growth of, and diffusion in, olivine in ultra-fast ascending basalt magmas from Shiveluch volcano. Scientific Reports, 8(1), 11,775.
- Grove, T., Elkins-Tanton, L., Parman, S., Chatterjee, N., Müntener, O., and Gaetani, G. (2003) Fractional crystallization and mantle-melting controls on cale-alkaline differentiation trends. Contributions to Mineralogy and Petrology, 145(5), 515–533.
- Grove, T.L., Baker, M.B., Price, R.C., Parman, S.W., Elkins-Tanton, L.T., Chatterjee, N., and Müntener, O. (2005) Magnesian andesite and dacite lavas from Mt. Shasta,

- northern California: products of fractional crystallization of H₂O-rich mantle melts. Contributions to Mineralogy and Petrology, 148(5), 542–565.
- Grove, T.L., Chatterjee, N., Parman, S.W., and Médard, E. (2006) The influence of H₂O on mantle wedge melting. Earth and Planetary Science Letters, 249(1–2), 74–89.
- Grove, T.L., Till, C.B., and Krawczynski, M.J. (2012) The role of H₂O in subduction zone magmatism. Annual Review of Earth and Planetary Sciences, 40(1), 413–439.
- Guggenheim, S., and van Groos, A.F.K. (2001) Baseline studies of the Clay Minerals Society Source Clays: Thermal analysis. Clays and Clay Minerals, 49(5), 433–443.
- Guillot, B., and Sarda, P. (2006) The effect of compression on noble gas solubility in silicate melts and consequences for degassing at mid-ocean ridges. Geochimica et Cosmochimica Acta, 70(5), 1215–1230. DOI: 10.1016/j.gca.2005.11.007
- Guillot, B., and Sator, N. (2012) Noble gases in high-pressure silicate liquids: A computer simulation study. Geochimica et Cosmochimica Acta, 80, 51–69. DOI: 10.1016/j. gca.2011.11.040
- Hacker, B.R. (2008) H₂O subduction beyond arcs. Geochemistry, Geophysics, Geosystems, 9(3), Q03001. DOI: 10.1029/2007GC001707
- Hacker, B.R., Abers, G.A., and Peacock, S.M. (2003) Subduction factory 1. Theoretical mineralogy, densities, seismic wave speeds, and H₂O contents. Journal of Geophysical Research: Solid Earth, 108(B1). DOI: 10.1029/2001JB001127
- Hamilton, D.L., Burnham, C.W., and Osborn, E.F. (1964) The solubility of water and effects of oxygen fugacity and water content on crystallization in mafic magmas. Journal of Petrology, 5(1), 21–39. DOI: 10.1093/petrology/5.1.21
- Hartley, M.E., Maclennan, J., Edmonds, M., and Thordarson, T. (2014) Reconstructing the deep CO₂ degassing behaviour of large basaltic fissure eruptions. Earth and Planetary Science Letters, 393, 120–131. DOI: 10.1016/j.epsl.2014.02.031
- Hartley, M.E., Neave, D.A., Maclennan, J., Edmonds, M., and Thordarson, T. (2015) Diffusive over-hydration of olivine-hosted melt inclusions. Earth and Planetary Science Letters, 425, 168–178. DOI: 10.1016/j.epsl.2015.06.008
- Hauri, E. (2002) SIMS analysis of volatiles in silicate glasses, 2: Isotopes and abundances in Hawaiian melt inclusions. Chemical Geology, 183(1–4), 115–141.
- Hauri, E., Wang, J., Dixon, J.E., King, P.L., Mandeville, C., and Newman, S. (2002) SIMS analysis of volatiles in silicate glasses: 1. Calibration, matrix effects and comparisons with FTIR. Chemical Geology, 183(1), 99–114.
- Herzberg, C.T., Fyfe, W.S., and Carr, M.J. (1983) Density constraints on the formation of the continental Moho and crust. Contributions to Mineralogy and Petrology, 84(1), 1–5. DOI: 10.1007/bf01132324
- Holtz, F., Sato, H., Lewis, J., Behrens, H., and Nakada, S. (2005) Experimental petrology of the 1991–1995 Unzen dacite, Japan. Part I: Phase relations, phase composition and pre-eruptive conditions. Journal of Petrology, 46(2), 319–337.
- Hughes, E.C., Buse, B., Kearns, S.L., Blundy, J.D., Kilgour, G., and Mader, H.M. (2019) Low analytical totals in EPMA of hydrous silicate glass due to sub-surface charging: Obtaining accurate volatiles by difference. Chemical Geology, 505, 48–56.
- Humphreys, M.C.S., Kearns, S.L., and Blundy, J.D. (2006) SIMS investigation of electron-beam damage to hydrous, rhyolitic glasses: Implications for melt inclusion analysis. American Mineralogist, 91, 667–679. DOI: 10.2138/am.2006.1936
- Humphreys, M.C.S., Menand, T., Blundy, J.D., and Klimm, K. (2008) Magma ascent rates in explosive eruptions: Constraints from H₂O diffusion in melt inclusions. Earth and Planetary Science Letters, 270(1), 25–40. DOI: 10.1016/j.epsl.2008.02.041
- Ihinger, P.D., Hervig, R.L., and McMillan, P.F. (1994) Analytical methods for volatiles in glasses. Reviews in Mineralogy and Geochemistry, 30, 67–121.
- Imae, N., and Ikeda, Y. (2007) Petrology of the Miller Range 03346 nakhlite in comparison with the Yamato-000593 nakhlite. Meteoritics & Planetary Science, 42(2), 171–184. DOI: 10.1111/j.1945-5100.2007.tb00225.x
- Ionov, D.A. (2010) Petrology of mantle wedge lithosphere: New data on supra-subduction zone peridotite xenoliths from the Andesitic Avacha Volcano, Kamchatka. Journal of Petrology, 51(1-2), 327–361. DOI: 10.1093/petrology/egp090
- Johnson, E.R., Wallace, P.J., Cashman, K.V., Granados, H.D., and Kent, A.J.R. (2008) Magmatic volatile contents and degassing-induced crystallization at Volcán Jorullo, Mexico: Implications for melt evolution and the plumbing systems of monogenetic volcanoes. Earth and Planetary Science Letters, 269(3–4), 478–487.
- Kamenetsky, V.S., Crawford, A.J., Eggins, S., and Mühe, R. (1997) Phenocryst and melt inclusion chemistry of near-axis seamounts, Valu Fa Ridge, Lau Basin: insight into mantle wedge melting and the addition of subduction components. Earth and Planetary Science Letters, 151(3), 205–223. DOI: 10.1016/S0012-821X(97)81849-3
- Kamenetsky, V.S., Sobolev, A.V., Eggins, S.M., Crawford, A.J., and Arculus, R.J. (2002) Olivine-enriched melt inclusions in chromites from low-Ca boninites, Cape Vogel, Papua New Guinea: evidence for ultramafic primary magma, refractory mantle source and enriched components. Chemical Geology, 183(1), 287–303.
- Katz, R.F., Spiegelman, M., and Langmuir, C.H. (2003) A new parameterization of hydrous mantle melting. Geochemistry, Geophysics, Geosystems, 4(9), 1073.
- Kayzar, T.M., Nelson, B.K., Bachmann, O., Bauer, A.M., and Izbekov, P.E. (2014) Deciphering petrogenic processes using Pb isotope ratios from time-series samples at Bezymianny and Klyuchevskoy volcanoes, Central Kamchatka Depression. Contributions to Mineralogy and Petrology, 168, 1067. DOI: 10.1007/s00410-014-1067-6
- Kent, A.J.R. (2008) Melt inclusions in basaltic and related volcanic rocks. Reviews in Mineralogy and Geochemistry, 69, 273–331. DOI: 10.2138/rmg.2008.69.8
- King, P.L., Vennemann, T.W., Holloway, J.R., Hervig, R.L., Lowenstern, J.B., and Forneris, J.F. (2002) Analytical techniques for volatiles: A case study using intermediate (andesitic) glasses. American Mineralogist, 87, 1077–1089.
- Knowlton, G.D., White, T.R., and McKague, H.L. (1981) Thermal study of types of water

- associated with clinoptilolite. Clays & Clay Minerals, 29(5), 403-411.
- Kohn, S.C., Henderson, C.M.B., and Mason, R.A. (1989) Element zoning trends in olivine phenocrysts from a supposed primary high-magnesian andesite: an electron- and ion-microprobe study. Contributions to Mineralogy and Petrology, 103(2), 242–252. DOI: 10.1007/bf00378510
- Krawczynski, M.J., and Olive, J.L. (2011) A new fitting algorithm for petrological mass-balance problems. 2011 Fall Meeting, AGU, San Francisco, Calif., 5-9 Dec, Abstract V53B-2613.
- Krawczynski, M.J., Grove, T.L., and Behrens, H. (2012) Amphibole stability in primitive are magmas: effects of temperature, H₂O content, and oxygen fugacity. Contributions to Mineralogy and Petrology, 164(2), 317–339. DOI: 10.1007/s00410-012-0740-x
- Kumamoto, K.M., Warren, J.M., and Hauri, E.H. (2017) New SIMS reference materials for measuring water in upper mantle minerals. American Mineralogist, 102, 537–547. DOI: 10.2138/am-2017-5863CCBYNCND
- Lees, J.M., Symons, N., Chubarova, O., Gorelchik, V., and Ozerov, A. (2007) Tomographic images of Klyuchevskoy Volcano P-wave velocity. In J. Eichelberger, E. Gordeev, P. Izbekov, M. Kasahara, and J. Lees, Eds., Volcanism and Subduction: The Kamchatka Region, 172, p. 293–302. American Geophysical Union.
- Levin, V., Droznina, S., Gavrilenko, M., Carr, M.J., and Senyukov, S. (2014) Seismically active subcrustal magma source of the Klyuchevskoy volcano in Kamchatka, Russia. Geology, 42(11), 983–986. DOI: 10.1130/g35972.1
- Lloyd, A., Plank, T., Ruprecht, P., Hauri, E., and Rose, W. (2013) Volatile loss from melt inclusions in pyroclasts of differing sizes. Contributions to Mineralogy and Petrology, 165(1), 129–153. DOI: 10.1007/s00410-012-0800-2
- Lloyd, A.S., Ruprecht, P., Hauri, E.H., Rose, W., Gonnermann, H.M., and Plank, T. (2014) NanoSIMS results from olivine-hosted melt embayments: Magma ascent rate during explosive basaltic eruptions. Journal of Volcanology and Geothermal Research, 283, 1–18. DOI: 10.1016/j.jvolgeores.2014.06.002
- Maclennan, J. (2017) Bubble formation and decrepitation control the CO₂ content of olivine-hosted melt inclusions. Geochemistry, Geophysics, Geosystems, 18(2), 597–616. DOI: 10.1002/2016GC006633
- Massare, D., Métrich, N., and Clocchiatti, R. (2002) High-temperature experiments on silicate melt inclusions in olivine at 1 atm: inference on temperatures of homogenization and H₂O concentrations. Chemical Geology, 183(1–4), 87–98.
- McGary, R.S., Evans, R.L., Wannamaker, P.E., Elsenbeck, J., and Rondenay, S. (2014) Pathway from subducting slab to surface for melt and fluids beneath Mount Rainier. Nature, 511(7509), 338–340. DOI: 10.1038/nature13493
- McMillan, P.F. (1994) Water solubility and speciation models. Reviews in Mineralogy and Geochemistry, 30, 132–156.
- Métrich, N., and Wallace, P.J. (2008) Volatile abundances in basaltic magmas and their degassing paths tracked by melt inclusions. Reviews in Mineralogy and Geochemistry, 69, 363–402. DOI: 10.2138/rmg.2008.69.10
- Métrich, N., Allard, P., Spilliaert, N., Andronico, D., and Burton, M. (2004) 2001 flank eruption of the alkali- and volatile-rich primitive basalt responsible for Mount Etna's evolution in the last three decades. Earth and Planetary Science Letters, 228(1), 1–17. DOI: 10.1016/j.epsl.2004.09.036
- Mielenz, R.C., Schieltz, N.C., and King, M.E. (1953) Thermogravimetric analysis of clay and clay-like minerals. Clays and Clay Minerals, 285–314.
- Mironov, N.L., and Portnyagin, M.V. (2011) H₂O and CO₂ in parental magmas of Kliuchevskoi volcano inferred from study of melt and fluid inclusions in olivine. Russian Geology and Geophysics, 52(11), 1353–1367. DOI: 10.1016/j.rgg.2011.10.007
- Mironov, N., Portnyagin, M., Botcharnikov, R., Gurenko, A., Hoemle, K., and Holtz, F. (2015) Quantification of the CO₂ budget and H₂O–CO₂ systematics in subduction-zone magmas through the experimental hydration of melt inclusions in olivine at high H₂O pressure. Earth and Planetary Science Letters, 425, 1–11.
- Mitchell, A.L., Gaetani, G.A., O'Leary, J.A., and Hauri, E.H. (2017) H₂O solubility in basalt at upper mantle conditions. Contributions to Mineralogy and Petrology, 172(10), 85. DOI: 10.1007/s00410-017-1401-x
- Moore, G. (2008) Interpreting H₂O and CO₂ contents in melt inclusions: Constraints from solubility experiments and modeling. Reviews in Mineralogy and Geochemistry, 69, 333–362. DOI: 10.2138/rmg.2008.69.9
- Moore, D., and Reynolds, R. Jr. (1997) X-ray Diffraction and the Identification and Analysis of Clay Minerals, 378 p. Oxford University Press.
- Moore, G., Vennemann, T., and Carmichael, I.S.E. (1998) An empirical model for the solubility of H₂O in magmas to 3 kilobars. American Mineralogist, 83, 36–42.
- Moore, L.R., Gazel, E., Tuohy, R., Lloyd, A.S., Esposito, R., Steele-MacInnis, M., Hauri, E.H., Wallace, P.J., Plank, T., and Bodnar, R.J. (2015) Bubbles matter: An assessment of the contribution of vapor bubbles to melt inclusion volatile budgets. American Mineralogist. 100(4), 806–823. DOI: 10.2138/am-2015–5036.
- Mysen, B. (2014) Water-melt interaction in hydrous magmatic systems at high temperature and pressure. Progress in Earth and Planetary Science, 1(1), 4.
- Nash, W.P. (1992) Analysis of oxygen with the electron microprobe: Applications to hydrated glass and minerals. American Mineralogist, 77, 453–457.
- Nowak, M., and Behrens, H. (1995) The speciation of water in haplogranitic glasses and melts determined by in situ near-infrared spectroscopy. Geochimica et Cosmochimica Acta, 59(16), 3445–3450. DOI: 10.1016/0016-7037(95)00237-T
- Nye, C.J., and Reid, M.R. (1986) Geochemistry of primary and least fractionated lavas from Okmok volcano, Central Aleutians: implications for arc magmagenesis. Journal of Geophysical Research, 91(B10), 10271–10287. DOI: 10.1029/JB091iB10p10271 Ochs. F.A., and Lange. R.A. (1999) The density of hydrous magmatic liquids. Science.

- 283(5406), 1314-1317. DOI: 10.1126/science.283.5406.1314
- Ozerov, A.Y. (2000) The evolution of high-alumina basalts of the Klyuchevskoy volcano, Kamchatka, Russia, based on microprobe analyses of mineral inclusions. Journal of Volcanology and Geothermal Research, 95(1–4), 65–79.
- ———(2009) Experimental modeling of the explosion mechanism of basaltic magmas. Petrology, 17(7), 653–668. DOI: 10.1134/s0869591109070029
- Ozerov, A.Y., Ariskin, A.A., Kyle, P., Bogoyavlenskaya, G.E., and Karpenko, S.F. (1997) Petrological-geochemical model for genetic relationships between basaltic and andesitic magmatism of Klyuchevskoi and Bezymyannyi volcanoes, Kamchatka. Petrology, 5(6), 550–569.
- Paonita, A. (2005) Noble gas solubility in silicate melts:a review of experimentation and theory, and implications regarding magma degassing processes. Annals of Geophysics, 48(4-5), 647–669. DOI: 10.4401/ag-3225
- Papale, P., Moretti, R., and Barbato, D. (2006) The compositional dependence of the saturation surface of H₂O+CO₂ fluids in silicate melts. Chemical Geology, 229(1), 78–95. DOI: 10.1016/j.chemgeo.2006.01.013
- Parai, R., and Mukhopadhyay, S. (2012) How large is the subducted water flux? New constraints on mantle regassing rates. Earth and Planetary Science Letters, 317-318, 396–406. DOI: 10.1016/j.epsl.2011.11.024
- Peslier, A.H., Schönbächler, M., Busemann, H., and Karato, S.-I. (2017) Water in the Earth's interior: distribution and origin. Space Science Reviews, 212(1), 743–810.Petrelli, M., El Omari, K., Spina, L., Le Guer, Y., La Spina, G., and Perugini, D. (2018)
- Fereini, M., El Omari, K., Spina, L., Le Guer, Y., La Spina, G., and Pertigini, D. (2016)
 Timescales of water accumulation in magmas and implications for short warning times of explosive eruptions. Nature Communications, 9(1), 770.
- Plank, T., Kelley, K.A., Zimmer, M.M., Hauri, E.H., and Wallace, P.J. (2013) Why do mafic arc magmas contain ~4 wt% water on average? Earth and Planetary Science Letters, 364, 168–179. DOI: 10.1016/j.epsl.2012.11.044
- Portnyagin, M., Hoernle, K., Plechov, P., Mironov, N., and Khubunaya, S. (2007) Constraints on mantle melting and composition and nature of slab components in volcanic arcs from volatiles (H₂O, S, Cl, F) and trace elements in melt inclusions from the Kamchatka Arc. Earth and Planetary Science Letters, 255(1–2), 53–69.
- Portnyagin, M., Almeev, R., Matveev, S., and Holtz, F. (2008) Experimental evidence for rapid water exchange between melt inclusions in olivine and host magma. Earth and Planetary Science Letters, 272(3–4), 541–552. DOI: 10.1016/j.epsl.2008.05.020
- Pozgay, S.H., Wiens, D.A., Conder, J.A., Shiobara, H., and Sugioka, H. (2009) Seismic attenuation tomography of the Mariana subduction system: Implications for thermal structure, volatile distribution, and slow spreading dynamics. Geochemistry, Geophysics, Geosystems, 10(4), Q04X05. DOI: 10.1029/2008GC002313
- Qin, Z., Lu, F., and Anderson, A.T. (1992) Diffusive reequilibration of melt and fluid inclusions. American Mineralogist, 77, 565–576.
- Rivalta, E., Taisne, B., Bunger, A.P., and Katz, R.F. (2015) A review of mechanical models of dike propagation: Schools of thought, results and future directions. Tectonophysics, 638, 1–42. DOI: 10.1016/j.tecto.2014.10.003
- Rubin, A.M. (1993) Tensile fracture of rock at high confining pressure: Implications for dike propagation. Journal of Geophysical Research: Solid Earth, 98(B9), 15,919–15,935. DOI: 10.1029/93JB01391
- Ruprecht, P., and Plank, T. (2013) Feeding andesitic eruptions with a high-speed connection from the mantle. Nature, 500, 68–72. DOI: 10.1038/nature12342
- Ruscitto, D.M., Wallace, P.J., and Kent, A.J.R. (2011) Revisiting the compositions and volatile contents of olivine-hosted melt inclusions from the Mount Shasta region: implications for the formation of high-Mg andesites. Contributions to Mineralogy and Petrology, 162(1), 109–132. DOI: 10.1007/s00410-010-0587-y
- Rutherford, M.J., and Devine, J.D. (1996) Preeruption pressure-temperature conditions and volatiles in the 1991 dacitic magma of Mount Pinatubo. Fire and mud: eruptions and lahars of Mt. Pinatubo, Philippines, p. 751–766. U.S. Geological Survey.
- Schiano, P. (2003) Primitive mantle magmas recorded as silicate melt inclusions in igneous minerals. Earth-Science Reviews. 63(1), 121–144.
- Schiano, P., and Bourdon, B. (1999) On the preservation of mantle information in ultramafic nodules: glass inclusions within minerals versus interstitial glasses. Earth and Planetary Science Letters, 169(1), 173–188. DOI: 10.1016/S0012-821X(99)00074-6
- Shishkina, T.A. (2012) Storage conditions and degassing processes of low-K and high-Al tholeiitic island-arc magmas: experimental constraints and natural observations for Mutnovsky volcano, Kamchatka. Naturwissenschaftliche Fakultät, Ph.D. thesis, 214 p. Leibniz Universität Hannover, Germany.
- Shishkina, T.A., Botcharnikov, R.E., Holtz, F., Almeev, R.R., and Portnyagin, M.V. (2010) Solubility of H₂O- and CO₂-bearing fluids in tholeiitic basalts at pressures up to 500 MPa. Chemical Geology, 277(1–2), 115–125.
- Shishkina, T.A., Botcharnikov, R.E., Holtz, F., Almeev, R.R., Jazwa, A.M., and Jakubiak, A.A. (2014) Compositional and pressure effects on the solubility of H₂O and CO₂ in mafic melts. Chemical Geology, 388, 112–129.
- Silver, L., and Stolper, E. (1989) Water in Albitic Glasses. Journal of Petrology, 30(3), 667–709. DOI: 10.1093/petrology/30.3.667
- Skirius, C.M., Peterson, J.W., and Anderson, A.T. (1990) Homogenizing rhyolitic glass inclusions from the Bishop Tuff. American Mineralogist, 75, 1381–1398.
- Sobolev, A.V., and Chaussidon, M. (1996) H₂O concentrations in primary melts from supra-subduction zones and mid-ocean ridges: Implications for H₂O storage and recycling in the mantle. Earth and Planetary Science Letters, 137(1), 45–55.
- Sommer, M.A. (1977) Volatiles H₂O, CO₂, and CO in silicate melt inclusions in quartz

- phenocrysts from the Rhyolitic Bandelier Air-Fall and Ash-Flow Tuff, New Mexico. The Journal of Geology, 85(4), 423–432. DOI: 10.1086/628316
- Steele-Macinnis, M., Esposito, R., and Bodnar, R.J. (2011) Thermodynamic model for the effect of post-entrapment crystallization on the H₂O–CO₂ systematics of vapor-saturated, silicate melt inclusions. Journal of Petrology, 52(12), 2461–2482.
- Steele-MacInnis, M., Esposito, R., Moore, L.R., and Hartley, M.E. (2017) Heterogeneously entrapped, vapor-rich melt inclusions record pre-eruptive magmatic volatile contents. Contributions to Mineralogy and Petrology, 172(4), 18.
- Stolper, E. (1982a) The speciation of water in silicate melts. Geochimica et Cosmochimica Acta, 46(12), 2609–2620. DOI: 10.1016/0016-7037(82)90381-7
- ———(1982b) Water in silicate glasses: An infrared spectroscopic study. Contributions to Mineralogy and Petrology, 81(1), 1–17. DOI: 10.1007/bf00371154
- Straub, S.M., and Layne, G.D. (2003) The systematics of chlorine, fluorine, and water in Izu arc front volcanic rocks: Implications for volatile recycling in subduction zones. Geochimica et Cosmochimica Acta, 67(21), 4179–4203.
- Straub, S.M., LaGatta, A.B., Martin-Del Pozzo, A.L., and Langmuir, C.H. (2008) Evidence from high-Ni olivines for a hybridized peridotite/pyroxenite source for orogenic andesites from the central Mexican Volcanic Belt. Geochemistry, Geophysics, Geosystems, 9(3), Q03007. DOI: 10.1029/2007GC001583
- Streck, M.J., and Leeman, W.P. (2018) Petrology of "Mt. Shasta" high-magnesian andesite (HMA): A product of multi-stage crustal assembly. American Mineralogist, 103(2), 216–240. DOI: 10.2138/am-2018-6151
- Stroncik, N.A., and Schmincke, H.-U. (2002) Palagonite—a review. International Journal of Earth Sciences, 91(4), 680–697. DOI: 10.1007/s00531-001-0238-7
- Taisne, B., and Jaupart, C. (2011) Magma expansion and fragmentation in a propagating dyke. Earth and Planetary Science Letters, 301(1), 146–152.
- Tolstykh, M.L., Naumov, V.B., Gavrilenko, M.G., Ozerov, A.Y., and Kononkova, N.N. (2012) Chemical composition, volatile components, and trace elements in the melts of the Gorely volcanic center, southern Kamchatka: Evidence from inclusions in minerals. Geochemistry International, 50(6), 522–550.
- van Keken, P.E., Hacker, B.R., Syracuse, E.M., and Abers, G.A. (2011) Subduction factory: 4. Depth-dependent flux of H₂O from subducting slabs worldwide. Journal of Geophysical Research: Solid Earth, 116(B1). DOI: 10.1029/2010JB007922
- Wallace, P.J. (2005) Volatiles in subduction zone magmas: concentrations and fluxes based on melt inclusion and volcanic gas data. Journal of Volcanology and Geothermal Research, 140(1–3), 217–240. DOI: 10.1016/j.jvolgeores.2004.07.023
- Wallace, P.J., Kamenetsky, V.S., and Cervantes, P. (2015a) Melt inclusion CO₂ contents, pressures of olivine crystallization, and the problem of shrinkage bubbles. American Mineralogist, 100, 787–794. DOI: 10.2138/am-2015-5029
- Wallace, P.J., Plank, T., Edmonds, M., and Hauri, E.H. (2015b) Chapter 7—Volatiles in Magmas. In H. Sigurdsson, Ed., The Encyclopedia of Volcanoes (2nd ed.), p. 163–183. Academic Press, Amsterdam.
- Walowski, K. (2015) From cinder cones to subduction zones: Volatile recycling and magma formation beneath the Southern Cascade Arc, p. 169. Ph.D. thesis, University of Oregon, Eugene, Oregon.
- Wanamaker, B.J., Wong, T.-F., and Evans, B. (1990) Decrepitation and crack healing of fluid inclusions in San Carlos olivine. Journal of Geophysical Research: Solid Earth, 95(B10), 15,623–15,641. DOI: 10.1029/JB095iB10p15623
- Weller, D.J., and Stern, C.R. (2018) Along-strike variability of primitive magmas (major and volatile elements) inferred from olivine-hosted melt inclusions, southernmost Andean Southern Volcanic Zone, Chile. Lithos, 296-299, 233–244.
- Zellmer, G.F., Edmonds, M., and Straub, S.M. (2015) Volatiles in subduction zone magmatism. Geological Society, London, Special Publications, 410(1), 1–17.
- Zellmer, G.F., Pistone, M., Iizuka, Y., Andrews, B.J., Gómez-Tuena, A., Straub, S.M., and Cottrell, E. (2016) Petrogenesis of antecryst-bearing arc basalts from the Trans-Mexican Volcanic Belt: Insights into along-arc variations in magma-mush ponding depths, H₂O contents, and surface heat flux. American Mineralogist, 101, 2405–2422. DOI: 10.2138/am-2016-5701
- Zhang, Y. (1998) Mechanical and phase equilibria in inclusion–host systems. Earth and Planetary Science Letters, 157(3), 209–222. DOI: 10.1016/S0012-821X(98)00036-3
- Zhang, H.L., Hirschmann, M.M., Cottrell, E., and Withers, A.C. (2017) Effect of pressure on Fe²⁺/ΣFe ratio in a mafic magma and consequences for magma ocean redox gradients. Geochimica et Cosmochimica Acta. 204. 83–103.
- Zimmer, M.M., Plank, T., Hauri, E.H., Yogodzinski, G.M., Stelling, P., Larsen, J., Singer, B., Jicha, B., Mandeville, C., and Nye, C.J. (2010) The role of water in generating the cale-alkaline trend: New Volatile data for Aleutian magmas and a new tholeiitic index. Journal of Petrology, 51(12), 2411–2444. DOI: 10.1093/petrology/egq062

MANUSCRIPT RECEIVED JULY 16, 2018
MANUSCRIPT ACCEPTED APRIL 9, 2019
MANUSCRIPT HANDLED BY KYLE ASHLEY

Endnote:

¹Deposit item AM-19-76735, Supplemental Materials. Deposit items are free to all readers and found on the MSA website, via the specific issue's Table of Contents (go to http://www.minsocam.org/MSA/AmMin/TOC/2019/Jul2019_data/Jul2019_data.html).